A Last Interglacial record of environmental changes from the Sulmona Basin (central Italy)

Eleonora Regattieri[*, 1, 2, 3], Biagio Giaccio[2], Sebastien Nomade[4], Alexander Francke[1], Hendrik Vogel[5], Russell N. Drysdale[6, 7], Natale Perchiazzi[8], Bernd Wagner[1], Maurizio Gemelli[8], Ilaria Mazzini[2], Chiara Boschi[3], Paolo Galli[9, 2]; Edoardo Peronace[2]

[1]Institute of Geology and Mineralogy, University of Cologne, Zülpicher Str. 49a, 50674 Cologne, Germany
[2]Istituto di Geologia Ambientale e Geoingegneria, IGAG-CNR, Via Salaria km. 29.4 Monterotondo Rome, Italy[2]
[3]Istituto di Geoscienze e Georisorse, IGG-CNR, Via Moruzzi 1, 56126 Pisa, Italy
[4]Laboratoire des Sciences du Climat et de l'Environnement, IPSL, laboratoire CEA/CNRS/UVSQ et Université de Paris-Saclay, Gif-Sur-Yvette, France
[5]Institute of Geological Sciences & Oeschger Centre for Climate Change Research, University of Bern, Switzerland
[6]School of Geography, University of Melbourne, Victoria 3010, Australia
[7]EDYTEM, UMR CNRS 5204, Université de Savoie-Mont Blanc, 73376 Le Bourget du Lac-Cedex, France
[8]Dipartimento di Scienze della Terra, University of Pisa, Via S. Maria 53, 56126 Pisa, Italy
[9]Dipartimento di Protezione Civile, Via Vitorchiano 4, 00189 Rome, Italy
*Corresponding author: Eleonora Regattieri regattieri@dst.unipi.it

Abstract

Here we present a multiproxy record ($\delta^{13}C$, $\delta^{18}O$, major and minor element composition, mineralogy, and low-resolution biogenic silica content) from a lacustrine succession in the Sulmona Basin, central Italy. Based on previous tephrochronological constraints and a new $^{40}Ar/^{39}Ar$ dating of a tephra matching the widespread X-6 tephra, the record spans the ca. 129-92 ka period and documents at sub-orbital scale the climatic and environmental changes over the Last Interglacial and its transition to the Last Glacial period. The $\delta^{18}O$ composition is interpreted as a proxy for the amount and seasonality of local precipitation, whereas variations in elemental and mineralogical composition are inferred to reflect climatic-driven changes in clastic sediment input. The observed variations are consistent among the different proxies, and indicate that periods of reduced precipitation were marked by enhanced catchment erosion, probably due to a reduction in vegetation cover. The first part of the Last Interglacial shows the most negative $\delta^{18}O$ values. Comparison with pollen records from the Mediterranean suggests a greater seasonality of the precipitation at this time. At millennial-to-centennial time scales, comparison of the Sulmona record with speleothem $\delta^{18}O$ records from central Italy highlights a highly coherent pattern of hydrological evolution, with enhanced variability and similar events of reduced precipitation consistently recorded by each isotope record. The observed intra-interglacial variability can potentially be linked, within the uncertainties associated with each age model, to similar variations observed in sea-surface

temperature records from the Mediterranean and the North Atlantic, suggesting a link between Mediterranean hydrology and North Atlantic temperature and circulation patterns that persists during periods of low ice volume.

Keywords: Paleoclimate; stable isotopes; lacustrine succession; tephrochronology

1. Introduction

The climate of the Last Interglacial (LIG), roughly corresponding to marine isotope stage (MIS) 5e and the Eemian interglacial in the European pollen stratigraphy (Govin et al., 2015 and references therein), has many features in common with model projections of future climate, because during this period much of the Earth experienced a climate warmer than present (e.g. Kukla et al., 2002). Although orbital parameters for MIS5e are quite different from that of the Holocene (e.g. Berger and Loutre, 1991), the LIG is a potential analog for projected future global warming and is thus an interesting study case for evaluating the climate and environmental responses during periods characterized by an excess of warmth. From this perspective, of particular interest are intra-interglacial millennial-scale climate changes. Evidence of abrupt climatic variations are well documented in several LIG records from North Atlantic marine sediments and Greenland ice (e.g. Oppo et al., 2001, 2006; Galaasen et al., 2014; Pol et al., 2014) and some seem to have propagated into the Mediterranean basin (Sánchez-Goñi et al., 1999; Martrat et al., 2004, 2014; Sprovieri et al., 2006; Kandiano et al., 2014). Potential expressions of this oceanic driven instability have also been recognized in central Europe (e.g. Sirocko et al., 2005; Seelos and Sirocko, 2007; Seelos et al., 2009), as well as in the Mediterranean region (e.g. Tzedakis et al., 2003; Brauer et al., 2007; Drysdale et al., 2007; Couchoud et al., 2009; Milner et al., 2013, 2016; Regattieri et al. 2014a, 2016a; Vogel et al., 2010; Lézine et al., 2010; Zanchetta et al., 2016). However, the effects of such changes on climate and ecosystems of the European continent are still poorly known and understood (Galaasen et al., 2014; Govin et al., 2015). Identification, correlation and evaluation of the climatic expressions of LIG millennial-scale variability outside the North Atlantic region remain unclear or largely based on postulated temporal phase relations. Addressing these issues requires the compilation of regionally representative, high-resolution and independently dated paleoclimatic records. Lacustrine successions deposited in tectonic basins of the Apennines are capable of fulfilling these requirements (Giaccio et al., 2015a, 2015b; Regattieri et al., 2015, 2016b; Russo-Ermolli et al., 2010) due to the high sensitivity of the local sediment properties, and particularly of the oxygen stable isotope composition of

64 authigenic carbonates ($\delta^{18}O$), to hydrological and environmental changes. Moreover, these archives offer
65 the possibility to develop independent age models based on the $^{40}Ar/^{39}Ar$ geochronometer that can be
66 directly or indirectly applied to the volcanic ash layers (tephra). These tephra layers, deriving from the
67 intense activity of Quaternary peri-Tyrrhenian explosive volcanism, are systematically found in the
68 lacustrine sediments of the Apennine intermountain basins (e.g. Giaccio et al., 2012; Petrosino et al.,
69 2014).
70 Of the central Italian continental basins, Sulmona has already been recognized as a promising archive.
71 The sedimentary record is underpinned by a robust tephrochronological framework (Giaccio et al., 2012,
72 2013a, 2013b), and provides important insights into climate and environmental evolution of the central
73 Mediterranean and the linkages with extra-regional climate variability (Giaccio et al., 2015a; Regattieri
74 et al., 2015, 2016b). In particular, the stable isotope profiles ($\delta^{18}O$ and $\delta^{13}C$), $CaCO_3$ content and
75 tephrostratigraphy of the Popoli section (POP hereafter), documenting Early Last Glacial climate
76 fluctuations (from ca. 115 to ca. 90 ka), highlight strong Mediterranean–North Atlantic climate
77 teleconnections as well as the influence of low-latitude circulation patterns (Regattieri et al., 2015). In
78 order to explore the environmental-hydrological changes over the entire early-to-middle MIS 5 (MIS 5e
79 to MIS 5c, ca. 129-92 ka), and in particular the intra-LIG millennial scale variability, in this study we
80 extended through a multiproxy approach ($\delta^{18}O$ and $\delta^{13}C$ analysis, $CaCO_3$ content, biogenic silica content,
81 XRF major and minor element composition, XRD-based bulk mineralogy and $^{40}Ar/^{39}Ar$ geochronology)
82 the investigation of the POP section back to ca.129 ka. The results provide a longer and richer multi-
83 proxy record, which allows a detailed reconstruction of local environmental change and give insights on
84 potential relations with the extra-regional millennial-scale variability during the full LIG and at the
85 LIG/Last Glacial transition.
86
87 **2. Study site**
88 ***2.1 Geological and stratigraphic setting***
89 An up-dating stratigraphic framework of the Sulmona Basin (Fig. 1) is provided in Giaccio et al. (2009
90 with amendments in Giaccio et al., 2013a; 2012), Galli et al. (2015) and Regattieri et al. (2015, 2016b),
91 to which the reader is referred for integrating the information summarized here. The Sulmona basin (Fig.
92 1) is a block-faulted intermontane depression which accumulated lacustrine sediments discontinuously
93 during the Quaternary (e.g. Cavinato et al., 1994; Cavinato and Miccadei, 1995, 2000; Miccadei et al.,
94 1998; Giaccio et al., 2012, 2013a). The exposed Pleistocene succession in the Sulmona basin is composed
95 of three main unconformity-bound, alluvial-fluvial-lacustrine units (SUL 6, SUL 5 and SUL 4-3),

chronologically constrained by magnetostratigraphy and tephrochronology (Giaccio et al., 2012, 2013a; 2013b; 2015a; Sagnotti et al., 2014, 2016). The interval investigated here (POP section) corresponds to the lowermost part of the SUL 4-3 unit (ca. 110-14 ka, Fig. 1). The outcropping portion of the POP section (~19 m from the top of the lacustrine deposits; Fig. 1) has been described by Giaccio et al. (2012), with particular attention to its tephrostratigraphy, and by Regattieri et al. (2015), who presented the stable isotope results ($\delta^{13}C$ and $\delta^{18}O$) from the lacustrine carbonates and extended the tephrostratigraphic investigation down to ~ 27 m of the outcrop depth (Fig. 1) by means of a trench and a borehole (Fig. 1).

Six tephras were previously recognised in the POP section, named from top to the base POP1, POP2, POP2a, POP2b, POP3 and POP4 (Fig. 1 and 2). Descriptions, tephrostratigraphic correlations with other archives and ages for these tephras have been provided by Giaccio et al. (2012) and Regattieri et al. (2015) and are summarized in Table 1. Here, we present a new $^{40}Ar/^{39}Ar$ age for tephra POP4, which chemically matches the X-6 tephra (Regattieri et al., 2015) of the marine tephrostratigraphic schemes of Keller et al. (1978). This tephra shows a large dispersal area covering the central Mediterranean and the Balkans (Bourne et al., 2015; Donato et al., 2016, Insinga et al., 2014, Iorio et al., 2014; Leicher et al., 2016; Lézine et al., 2010; Petrosino et al., 2016; Sulpizio et al., 2010; Vogel et al., 2010).

2.2 Climatic and hydrological settings

The Sulmona Basin is located in the central Apennines (Fig. 1) at a mean elevation of ~ 400 m a.s.l. The current mean annual temperature is 13.7 °C and the mean annual rainfall is 870 mm (data from the Sulmona meteorological station). About 60% of the region's precipitation has a North Atlantic origin, especially during winter, whereas the other 40% is mainly sourced from the western Mediterranean (Bard et al., 2002). The present hydrology of the basin is dominated by large perennial springs fed by the extensive karst systems hosted in the mountains surrounding the basin, where precipitation reaches values of about 1200 mm/yr at the summits. These springs are mainly fed by recharge at 1200-1500 m a.s.l. with minor input from higher altitudes (up to 2900 m a.s.l., Barbieri et al., 2005; Desiderio et al., 2005 a, b). Because they are recharged at higher altitude, the springs have a $\delta^{18}O$ composition lower than local precipitation (which is ~-7.13‰, data from L'Aquila station, Longinelli and Selmo, 2003). Discharge is higher during early spring due to snowmelt, lowering further the average $\delta^{18}O$ isotopic values of water recharging the basin (Falcone et al., 2008). Waters also have a higher $\delta^{13}C$ of dissolved inorganic carbon (DIC) compared with that of the more superficial springs due to longer water residence times and rock-water interactions within the karst (Falcone et al., 2008). These springs represented the main source also for the studied palaeo-lake and likely hydrological conditions of the high-altitude

127 catchment area dominated its recharge both during drier and wetter periods (Regattieri et al., 2015,
128 2016b; Giaccio et al., 2015a).
129

130 **3. Material and Methods**

131 ***3.1 Stratigraphy, sampling and stable isotope analyses***

132 In the current study we present new results from a ~13.1 m-thick lacustrine interval recovered in the
133 upper part of the ~ 60 m borehole described by Regattieri et al. (2015), which extends to ~40 m of the
134 outcrop depth of the previous investigation (Fig. 1). At this depth (corresponding to ~23 m in core, Fig.
135 1), the lacustrine succession is interrupted by a hydromorphic paleosol with an upper Histic horizon,
136 which marks the lowermost horizon investigated here. Below this peodogenic horizon (~1 m deep), the
137 sedimentary succession continues, first with a thin layer of gravel and then, continuously to the core
138 bottom, with greyish-greenish lacustrine-palustrine marls (Fig. 1). However, there are no chronological
139 constraints to allow us to define either the length of the sedimentary hiatus (represented by a paleosol
140 and gravel) or the age of the underlying lacustrine-palustrine sediments, which could be tentatively
141 attributed to a generic MIS 6 (Fig. 1). Thus, the interval below the peat layer is not discussed further.
142 The core was sampled at a resolution of ~10 cm between 26.9 m and 31.5 m and of ~5 cm between 31.5
143 and 39.9 m of the outcrop depth (a total of 13.1 m), which together correspond to the interval between
144 ~10.2 and ~23.3 m of the core depth (Fig. 1). Samples for stable isotope analyses were prepared following
145 the procedure described in Regattieri et al. (2015, 2016b). Measurements were made with an Analytical
146 Precision AP2003 continuous-flow isotope-ratio mass spectrometer (IRMS) at the University of
147 Melbourne, Australia, using the same method as described in Regattieri et al. (2015). Briefly, samples
148 were digested in 105% phosphoric acid at 70°C. Mass spectrometric measurements were made on the
149 evolved CO_2. Results were normalized to the Vienna Pee Dee Belemnite scale using an internal working
150 standard (NEW1, a Carrara Marble), calibrated against the international standards NBS18 and NBS19.
151 Average analytical precision on internal standards was ± 0.10‰ and ± 0.05‰ for $\delta^{18}O$ and $\delta^{13}C$
152 respectively.
153

154 ***3.2 Elemental and mineralogical analyses***

155 X-ray fluorescence spectrometry (XRF) and X-ray powder diffraction (XRPD) analyses were performed
156 at the Earth Sciences Department of the University of Pisa (Italy) using leftover powders of the stable
157 isotope analyses. XRF analyses were conducted at a resolution of ~25 cm. A NITON XL3t GOLDD +

158 hand-held XRF unit (HHXRF) was used. Characteristics and performance of the NITON XL3t is
159 described in Gemelli et al. (2014) and the analytical procedure for sediment samples in Regattieri et al.
160 (2016b).
161 X-ray powder diffraction (XRPD) analyses were performed on 23 unevenly spaced samples (Fig. 2),
162 using a Bruker D2 Phaser diffractometer equipped with a Lynxeye fast detector. Diffraction patterns
163 were analysed with the Bruker DIFFRAC-EVA software, both for phase identification and for semi-
164 quantitative estimation of mineral abundances through the comparison of measured peak areas.
165 Field Emission Scanning Electron Microscopy (FESEM) imaging of three samples (Fig. 2) was
166 performed with a Bruker QUANTA FEG 450 housed at the Department of Civil and Industrial
167 Engineering of the University of Pisa,
168
169 ***3.3 Biogenic Silica and sedimentological analyses***
170 Biogenic silica (bSi) concentrations were measured using Fourier transform infrared spectroscopy
171 (FTIRS) at the Institute of Geological Sciences, University of Bern, Switzerland using the method
172 described in Vogel et al. (2008) and Rosén et al. (2010). Calibration followed Meyer-Jacob et al. (2014).
173 Approximately 0.011 ± 0.0001 g of powdered sample was mixed with 0.500 ± 0.0005 g of oven-dried
174 spectroscopic grade potassium bromide (KBr, Uvasol®, Merck Corp.) and subsequently homogenized
175 using a mortar and pestle. A Bruker Vertex 70 equipped with a liquid-nitrogen-cooled MCT (mercury–
176 cadmium–telluride) detector, a KBr beam splitter, and a HTS-XT accessory unit (multisampler) was
177 used. Each sample was scanned 64 times at a wavenumber resolution of 4 cm^{-1} (reciprocal centimeters)
178 for the wavenumber range 520 to 3750 cm^{-1} in diffuse reflectance mode. FTIR spectra were normalized
179 using a linear baseline correction by setting two defined points of the recorded spectrum to zero (3750
180 and 2210 - 2200 cm^{-1}, respectively) prior to extracting information on bSi concentrations. Estimates of
181 accuracy and precision of the method are provided in Meyer-Jacob et al. (2014) and Vogel et al. (2016).
182 ***3.4 $^{40}Ar/^{39}Ar$ dating and age modelling***
183 A bulk sample of POP4 tephra was collected at the base of the trench described by Regattieri et al. (2015)
184 and dated by $^{40}Ar/^{39}Ar$ methods to obtain an independent age. Twenty pristine sanidine crystals in the
185 size range 300-400 μm were handpicked under a binocular microscope. To remove the attached
186 groundmass, they were slightly leached for 5 min in 7% HF acid. A total of 20 crystals were loaded in a
187 single pit hosted in an aluminum disk and irradiated for 30 min (Irr 95) in the B1 tube of the OSIRIS

reactor (French Atomic Energy Commission, Saclay, France). After irradiation, 13 single crystal were transferred into individual pit hosted in a copper sample holder and then loaded into a differential vacuum Cleartran© window. After slight leaching using a 25% W CO_2 laser (Synrad©) at 3.0% of the full laser power, the 13 individual sanidine crystals were fused at about 12% of the full laser power. The Ar isotopes were analyzed using a VG5400 mass spectrometer equipped with a single ion counter (Balzers© SEV 217 SEN), following the procedures outlined in Nomade et al. (2010). Neutron fluence (J) was monitored by co-irradiation of Alder Creek sanidine standard (ACS-2, Nomade et al., 2005). The J value was determined from analyses of three ACS-2 single grains and calculated using an age of 1.193 Ma (Nomade et al., 2005), and the total decay constant of Steiger and Jäger (1977) (i.e., J= $3.515\ 10^{-4} \pm 1.410\ 10^{-6}$). Mass discrimination was assessed by analysis of Air pipette throughout the analytical period, and was calculated relative to a $^{40}Ar/^{36}Ar$ ratio of 298.56 (Lee et al., 2006). Several proposed calibrations of the $^{40}Ar/^{39}Ar$ chronometer are currently in use, yielding ages that vary by ~1% (Kuiper et al., 2008; Renne et al., 2011; Jicha et al., 2016). This implies a difference in the calibrated age for our samples within the reported total uncertainty. However, because previous $^{40}Ar/^{39}Ar$ ages have been published using these values (Regattieri et al., 2015, 2016b), we chose to keep them for the current investigation. Procedural blanks were measured every two or three unknowns, depending on the sample beam size previously measured. For a typical 10-min static blank, the backgrounds were generally about 2.0-2.2 10^{-17} and 5.0-6.0 10^{-19} mole for ^{40}Ar and ^{36}Ar, respectively. Full analytical procedures are described in Nomade et al. (2010).

The age model (Fig. 3) and corresponding 95%-confidence limits were calculated with Clam 2.0 software (Blaauw, 2010), written in the open-source statistical environment R (R Development Core Team, 2010). Tephra ages in years before present (Table 1) were used and a smoothing-spline function was applied for interpolation between each age control point. Smoothing was set to 0.7 in CLAM (a smoothing of 0 is used for variable sedimentation rate, which produces a very flexible age model, whereas a smoothing of 1 equals linear interpolation between ages, corresponding to constant sedimentation rate). The age control points (tephra layers) in the upper part of the sequence do not indicate major changes in sedimentation rate. Because lithological information does not imply distinct shifts in sedimentation rate (i.e., the lithology is homogeneous throughout the succession), both in the upper and lower parts, for parts of the section where age control points are lacking, the age-depth modeling was calculated under the assumption of rather stable sedimentation rates (smoothing = 0.7) for the whole sequence (cf. Fig. 3).

4. Results and discussion

4.1 $^{40}Ar/^{39}Ar$ dating and chronology

Full analytical details for the 13 individual crystals analyses are given in Supplementary Table S1. Age-probability density spectra with individual single crystal age are presented Fig. 3. Among the 13 crystals analyzed, ten yielded a similar age. These juvenile crystals allowed calculation of a weighted mean age of 109.5 ± 0.9 ka (2σ analytical uncertainty, P = 0.94).

The age model provided in Fig. 3 is based on the tephra layers discussed previously by Giaccio et al. (2012) and Regattieri et al. (2015). Ages for five of these six tephra layers are the same as those used for the age model of Regattieri et al. (2015) (Table 1). For tephra POP4, the new $^{40}Ar/^{39}Ar$ age of 109.5 ± 0.9 ka is employed. Due to the difference between the new direct (109.5 ± 0.9 ka) and indirect (108.9 ± 1.8 ka; Iorio et al., 2014) $^{40}Ar/^{39}Ar$ ages of the POP4/X-6 tephra, and the different age-modeling approaches, the updated age model for the published section is slightly different from the previous model. However, both models are statistically indistinguishable, as all the differences are well within the associated uncertainties. The new age model spans from 92.5 ± 4.8 ka to 129.2 ± 6.9 ka and the resulting average temporal resolution of the record is ~90 years (from 91.7 ka to 121.6 ka) and ~50 years (from 121 ka to 130.0 ka) for stable isotope series, ~250 years for XRF results, and ~1 kyr for bSi. The relatively large uncertainty in the bottom part of the record is due to the lack of control points below the tephra POP4. Consequently, between ca. 110 and ca. 129 ka the age model is statistically extrapolated under the assumption of rather constant sedimentation rate (see Methods). To support our approach, it is worth mentioning that at Sulmona a rather stable sedimentation rate was observed also during the well-dated MIS 19 period; with no major changes between the full interglacial and the glacial inception (max 19% of variations for the ca. 770 - 758 ka interval, cf. Fig. 1 of Giaccio et al., 2015). Moreover, ongoing stratigraphic and chronological investigations on other intervals of the Sulmona succession also suggest rather constant sedimentation for the MIS 11 and the MIS 13 intervals (our unpublished data).

4.2 Lithology and mineralogy

As for the previously studied interval (Regattieri et al., 2015), the core is composed of greyish-to-whitish, faintly-to-well-bedded calcareous marl ($CaCO_3$ content between 80% and 20%, following the classification by Freytet and Verrecchia, 2002). FESEM investigations indicate that the carbonate fraction is mainly composed of euhedral to sub-euhedral calcite crystals of ~3-5 μm (Fig. 2). The size and morphology of the crystals are typical of authigenic calcite, i.e. of carbonates precipitated directly

from DIC of the lake water, mostly through algal fixation of CO_2, influenced by physical conditions, such as hydrology and temperature (e.g. Kelts and Hu, 1978; Talbot, 1990; Kelts and Talbot, 1990; Leng and Marshall, 2004, Gierlowski-Kordesch, 2010). FESEM investigations also show an abundance of diatom remains and rare, rounded, coarser clasts of quartz (Fig 2). Freshwater shells and ostracods (Mazzini et al., *in prep*.) are also present throughout the core, demonstrating the continuity of lacustrine conditions. Carbonate coatings and/or calcareous *charophytes* remains were not detected, suggesting that coring site was not influenced by littoral conditions. Overall, the lithology of the whole POP succession is highly homogeneous, suggesting that no major changes in the deposition environment happened during the covered time interval. Organic matter is virtually absent in the outcropping interval, due to subaerial oxidation, and is <1% wt for the core section. X-ray diffraction (XRD) analyses (Fig. 2) reveal that the prominent mineral phase in all samples is calcite, followed by minor quartz. Low-angle low-intensity XRD peaks indicate the presence of very minor amounts of phyllosilicates. In one sample, occurring at 127.5 ka, traces of gypsum were found.

4.3 The $\delta^{18}O$ record and its paleohydrological significance

4.3.1 Background

Stable isotope composition of oxygen ($\delta^{18}O$) of continental carbonates (lacustrine marl and speleothem) depends on isotopic composition of the precipitating solution (drip or lake water) and deposition temperature (e.g. Kim and O'Neil, 1997). According to the main processes supposed to affect the oxygen isotope fractionation, the $\delta^{18}O$ of carbonates is assessed as a proxy for paleotemperature and paleorainfall amount. The latter is considered to be the dominant process driving $\delta^{18}O$ in the Mediterranean region (e.g. Bar-Matthews et al., 2000, 2003; Bard et al., 2002; Zanchetta et al., 2007a, 2014, 2016a), together with precipitation/evaporation (P/E) ratio in lacustrine settings (e.g. Roberts et al., 2008; Zanchetta et al., 1999, 2007b, 2012). Carbonate $\delta^{18}O$ records from the central Mediterranean region also tend to show overall similarities with North Atlantic marine-sediment and Greenland ice-core records, indicating a strong teleconnection between North Atlantic temperature and ocean circulation patterns and Mediterranean hydrology (Drysdale et al., 2004, 2005, 2006, 2007, 2009; Regattieri et al., 2014a, b, 2016a, 2016b; Zanchetta et al., 2012 , 2014, 2016a, b). It has also been proposed that the hydrological significance of $\delta^{18}O$ of Mediterranean continental carbonates can be offset by the effects of changes in the isotopic composition of the sea source (Rohling et al., 2015; Marino et al., 2015). This effect can be

particularly important during major climatic shift, such as a deglaciation, when the decrease in planktonic $\delta^{18}O$ due to ice melting precedes the rise in sea-surface temperature (SST). However, multi-proxy studies from lake sediments and speleothems show variations in recharge-sensitive chemical and lithological properties synchronous with $\delta^{18}O$ changes, confirming the hydrological significance of $\delta^{18}O$ (Drysdale et al., 2009; Regattieri et al., 2016a, 2016b). Another factor which can affect the final $\delta^{18}O$ of continental carbonates is change in the relative proportion of Mediterranean (^{18}O-enriched) versus North Atlantic (^{18}O-depleted) precipitation. During cold periods, the strengthening of the north-westerly wind system would cause strong airflows through the passages between the Pyrenees, the Massif Central and the Alps, carrying cold and dry polar or continental air masses to the Gulf of Lyon. This favors cooling and evaporation of surface water masses in the western Mediterranean, leading to enhanced formation of Western Mediterranean Deep Water (WMDW) and stronger thermohaline circulation in the basin (Cacho et al., 2000). This mechanism acts in an opposite direction with respect to North Atlantic, where marine records indicate a reduced MOC during cold periods (e.g. Rasmussen et al., 1996; Curry and Oppo, 1997; Vidal et al., 1997). A higher proportion of vapor masses forming within the Mediterranean would have produced precipitation with higher $\delta^{18}O$, owing to reduced rainout fractionation and evaporation from a more isotopically enriched water mass compared to the North Atlantic. This fact has been also noted in several studies of present day precipitation (e.g. Celle-Jeanton et al., 2001). On the other hand, during warm periods WMDW formation is depressed while MOC is enhanced, leading to greater evaporation from the more isotopically depleted North Atlantic. This would produce a higher proportion of meteoric precipitation, having lower $\delta^{18}O$ values, exacerbated due to the higher rainout fractionation.

In previous studies on lacustrine carbonates from the Sulmona Basin, the $\delta^{18}O$ composition was interpreted as a proxy for precipitation amount in the high-altitude catchment of the karst recharge system (Giaccio et al., 2015a; Regattieri et al., 2015, 2016b), with higher (lower) $\delta^{18}O$ values related to drier (wetter) conditions. The influence on the final $\delta^{18}O$ of local precipitation and evaporation directly within the lake are considered to be of little relevance due to the large discharge of the karstic springs feeding the lake. On the other hand, increased evaporation under drier conditions favors the deposition of lake carbonates with higher $\delta^{18}O$ values, thus acting in the same direction of the amount effect.

Due to the extensive outcrop of carbonate bedrock in the Sulmona watershed (Fig. 1), it may be argued that detrital carbonate from the catchment may constitute an important component of the sediment. This would imply that changes in the clastic input could affect the $\delta^{18}O$ composition of the bulk sediment independently of the hydrological signal discussed above (e.g. Leng et al., 2010). Following the recommendations of Roberts et al. (2008), to exclude such contamination catchment carbonate rocks

need to be sampled and measured isotopically for comparison. In previous work on Sulmona spanning the MIS12-MIS11 interval, the comparison of isotope values from lacustrine marls and gravels from cores and nearby outcrops of marine carbonate bedrock shows that there is no significant mixing between detrital and authigenic calcite (Regattieri et al., 2016b). In Figure 4, $\delta^{18}O$ values for the MIS5 interval are reported along with those from the MIS12-11 interval (Regattieri et al., 2016b) and from the MIS19 interglacial (Giaccio et al., 2015a). These data are compared with isotope values of gravels from the Sulmona basin and carbonate alluvial deposits from the nearby Valle Giumentina (Villa et al., 2016), which drains the same Meso-Cenozoic carbonate domain. This extended comparison confirms the previous results: isotope values from the lacustrine carbonates can be readily discriminated from those of the catchment (Fig. 4), thus supporting the hypothesis that the authigenic calcite $\delta^{18}O$ signal dominates even when the clastic fraction is abundant, and that the variations observed are not due to mixing between allogenic (clastic) and authigenic (bio-meditated) carbonate.

Previously, the millennial variability of the $\delta^{18}O$ record of the POP section for the ca. 90-115 ka interval (Regattieri et al., 2015) was shown to be consistent with the patterns of Greenland Interstadials (GI) 25 to 23 (NGRIP members, 2004) and North Atlantic cold events C24–C23 (McManus et al., 2004), indicating a close phase relationship between the early Last Glacial paleoclimate variability of both regions. The POP record for the early Last Glacial also shows a prominent interval of negative $\delta^{18}O$ values corresponding to the GI24 event (108.0-105.1 ka). The higher amplitude of this oscillation, with respect to the Greenland $\delta^{18}O$ record and to speleothem $\delta^{18}O$ records from the Alps, both interpreted in terms of temperature (NALPS, Boch et al., 2008), was suggested to be related to enhanced seasonality of the climate (dry summer and wet winter) causing an annual bias toward ^{18}O-depleted winter precipitation and thus more negative calcite $\delta^{18}O$ (Regattieri et al., 2015).

4.3.2 The 115-129 ka $\delta^{18}O$ record

Stable isotope results plotted versus depth and versus age are presented in Fig. 2 and 5, respectively.

In this new presented interval (~27 to 40 m of the outcrop depth, Fig. 1; from 117.8 to 129.2 ka, Fig. 2 and 5), $\delta^{18}O$ ranges from -10.58 ‰ and -7.68 ‰. The $\delta^{18}O$ record starts with more negative values, which, based on the above-mentioned interpretation, indicate enhanced precipitation and potentially stronger seasonality lasting until 127.3 ka. Between 127.3 ka and 126.3 ka an abrupt rise in isotope values is related to decreasing precipitation and/or decreasing seasonality. It is followed by two short (~0.5 kyr) wetter reversals centred at 126.2 ka and 125.3 ka and by a steep trend of increasing values until ca. 125

343 ka. From ca.125 to 117.8 ka the record shows higher but more stable $\delta^{18}O$ values (Fig. 5). Less prominent
344 and shorter events (~ 0.5-1 kyr) of reduced precipitation are apparent at 122.7 ka, 119.1 ka, and 116.0 ka
345 (Fig. 5). It is worth mentioning that the ages attributed to these events are limited by the uncertainties
346 associated with the age model. However, such uncertainties affect to a lesser extent the age differences
347 and therefore the length and the temporal spacing of these short climatic events.

348

349 ***4.4 The carbon isotope record***

350 In the newly presented interval, the $\delta^{13}C$ ranges from -4.35‰ to -1.57‰, with a mean value of -3.41‰
351 (Figs. 2 and 5). The record starts with an interval of values around -3 ‰ and with a high multi-decadal
352 to centennial-scale variability. At ca. 126 ka there is an abrupt, brief positive excursion, followed by a
353 steep decrease until ca. 122 ka, after which values remain relatively stable before the marked dry interval
354 correlated to the C24 ocean cooling event at ca. 110 ka (Regattieri et al. 2015), but with brief low-
355 amplitude increase at ca. 116 ka (Fig. 5).
356 Factors influencing the isotopic composition of DIC in karstic lakes are numerous (Hollander and
357 McKenzie, 1991; Leng and Marshall, 2004; Mayer and Schwark, 1999; Zanchetta et al., 2012). In
358 general, ^{13}C-depleted intervals reflect an increased input of CO_2 derived from oxidation of organic matter
359 within the lake and/or leaching of soil-derived CO_2 from the catchment (e.g. Mook and Tan, 1991). On
360 the other hand, higher $\delta^{13}C$ values suggest increasing equilibration with atmospheric CO_2 and/or
361 contribution from bicarbonate originating from the dissolution of limestone, and/or increased ^{12}C
362 consumption by biological activity within the lake (e.g. Zanchetta et al., 2012). Influencing most of these
363 above-mentioned factors are variations in hydrological conditions, such as changes between open and
364 closed system. These are key drivers for changes in $\delta^{13}C$ composition (e.g. Roberts et al., 2008) and need
365 to be addressed thoroughly before to make any attempt to interpret the $\delta^{13}C$ record in terms of past climate
366 variability. However, Sulmona is a paleo-lake, so past hydrology is difficult to constrain and cannot be
367 fully inferred from present-day conditions. Thus, we stress that the interpretation of the $\delta^{13}C$ record
368 proposed here is based on current theory in the context of local physical setting. In the majority of the
369 interval previously discussed by Regattieri et al. (2015), from ca. 98 to 110 ka, and in the new record
370 back to ca. 122 ka, the $\delta^{13}C$ closely tracks $\delta^{18}O$ (Fig. 5). It may suggest that the evolution of the DIC of
371 the lake follows regional precipitation changes and the local E/P ratio. Covariations between $\delta^{18}O$ and
372 $\delta^{13}C$ in fact can be explained by: *i)* changes in soil development/productivity, promoted by rainfall-

induced vegetation cover changes, and thus by changes in the amount of soil CO_2 entering in the karst system (e.g. Lézine et al., 2010); or *ii)* to increased water residence time in the lake, which promotes evaporation (causing ^{18}O-enrichment) and equilibration of the DIC with atmospheric CO_2 (causing higher ^{13}C). The $\delta^{13}C$ record between ca. 129 ka and ca. 122 ka instead decouples from the $\delta^{18}O$. In detail, it is possible to define two intervals within this period: from 129.2 ka to ca. 125 ka mean $\delta^{13}C$ values are higher (Fig. 5) with respect to the subsequent portion of the LIG. However, there is a decreasing trend which mimics that of the $\delta^{18}O$, with a covariant increase at ~ca. 127.3 ka. Conversely, at the centennial scale, the two curves are anti-correlated (Fig. 4). For the period between ca.125 ka and ca. 122 ka, by contrast, the $\delta^{13}C$ values decrease rapidly and the anti-correlation with $\delta^{18}O$ is more persistent. Lower $\delta^{13}C$ values for the interval ca. 129-125 ka can potentially be explained by a muted soil development, and thus by a low amount of CO_2 from OM respiration/oxidation, in the high altitude recharge area of the karst system. A delayed development of soils in high altitude sites at the beginning of interglacial periods has already been inferred from speleothems $\delta^{13}C$ records from Corchia Cave in central Italy, both for the LIG (Drysdale et al., 2005, 2009, Fig. 5) and for the Holocene (Zanchetta et al., 2007a). The lag observed in the POP record is comparable to that of Corchia (2-3 kyr), as is the altitude of the recharge areas of the two sites (1200-1500 for Sulmona and ~1200 m a.s.l. for Corchia). Also at Sulmona, it is likely that glacier cover and erosion and/or sparse alpine vegetation cover may have hampered soil development during the early LIG, leading to a persistent contribution of ^{13}C-enriched atmospheric and bedrock carbon to the dissolved load of the karst aquifers. The short-term anti-correlation is more difficult to address. One likely candidate is that it is related to short-term increases in the proportion of waters originating from the karst system. Indeed, increased precipitation in the mountains (^{18}O-depleted) could trigger periods of karst system overflow, with injections of waters loaded with enriched $\delta^{13}C$ that originated from intermittently active sectors of the recharge system, which supply older water having longer interactions with the bedrock.

4.5 Elemental and mineralogical composition of the sediment

4.5.1 XRF

The depth and temporal series of the analyzed elements (Ti, Rb, Zr, Al, Si, Ca, Sr,) are shown in Fig. 2 and 6, respectively. Correlation coefficients are reported in Table 2 while scatterplots are reported in supplementary Fig. S1.

Ti, Rb, Zr, Al and Si variations are commonly linked to siliciclastic/detrital input to the lake and are associated also with grain-size variations (Koinig et al. 2003; Kylander et al., 2011; Vogel et al., 2010).

405 They are usually considered as proxies for the intensity of wind (Zr) and/or of erosion in the lake
406 catchment (Ti, Rb, Al, Si), increases of which are usually related to a reduction in vegetation cover, an
407 increase in soil erosion, and/or increased wind intensity (e.g. Vogel et al., 2010; Kylander et al., 2011).
408 Increases in all of these elements can also result from a closer proximity of the shoreline to the coring
409 site, i.e., a lower lake level, which also indicates drier climatic conditions. However, an increase in these
410 elements could be also related to increased runoff under wetter conditions (e.g. Francke et al. 2016).
411 At Sulmona, the lake catchment is mostly composed of carbonate rocks containing only a limited amount
412 of siliciclastic components, which are enriched in elements such as Ti, Rb, Zr, Al and Si. Thus, the most
413 likely source of these elements is volcanoclastic deposits, which are abundant in the whole basin (e.g.
414 Giaccio et al., 2009, 2012, 2013a), as well as small outcrops of Miocene-lower Pleistocene siliciclastic
415 flysch in the NW sector of the basin (Cavinato and Miccadei, 2000), and/or exotic aeolian dust. Si can
416 also be influenced by the presence of biogenic silica (bSi), which is the main component of diatom
417 frustules, and ranges from 13% wt to 2% wt in the studied interval (Section 4.6). Ca occurs mostly as
418 authigenic calcite, as revealed by XRD and FESEM analyses (Fig. 2 and Section 4.2.1). Thus, Ca content
419 can be seen as an indirect proxy for lake primary productivity. Sr can be either transported along with
420 the detrital fraction, as it is abundant in volcanoclastic deposits, or may substitute Ca in carbonates. The
421 low negative correlation of Sr with Ti, Zr, Rb and Si (Table 2, *r* values ranging from -0.25 to -0.35) and
422 the weak positive correlation between Sr and Ca (r=0.17) indicate that the Sr content is at least partly
423 related to either detrital input or co-precipitated as a divalent ion replacement for Ca in authigenic and
424 biogenic calcite.
425 Ti, Rb, Si, and Zr all show strong positive correlations (*r* values ranging from 0.86 and 0.97, Table 2)
426 and a similar trend of increasing values throughout the record (Fig. 6). However, the agreement between
427 these elements must be evaluated by considering the dilution effect related to the decreasing trend of
428 $CaCO_3$, which ranges from 85% to 40% from the base to the top of the sequence. Variations in Ca content,
429 which is mostly related to calcite precipitation, can affect the relative concentrations measured for other
430 elements and, as a matter of fact, Ca is strongly negatively correlated with all the above mentioned
431 elements (*r* values ranging from -0.67 and -0.85, Table 2). However, it is important to note that these
432 negative correlations are not an analytical artifact: they are consistent with climate-driven processes.
433 Colder and drier conditions trigger an increase in detrital input due to enhancement of soil erosion
434 promoted by reduced vegetation cover, leading to dilution of the $CaCO_3$ content. In addition, the
435 precipitation of authigenic carbonates, which is at least partly controlled by water temperature and
436 primary productivity, is reduced under conditions of climate deterioration. For example, cooler lake

437 waters hold more CO_2 and dissolved $CaCO_3$ in solution than warmer lake waters, and generally have a
438 lower ionic strength due to decreased dissolution rates in the catchment. This culminates in lower levels
439 of carbonate ion activity and supersaturation during cold stages, leading to lower rates of calcite
440 precipitation. Conversely, wetter and warmer periods promote denser vegetation cover and enhanced soil
441 development, reducing detrital flux from the catchment, and also increased lake primary productivity,
442 and increased rates of CO_2 degassing, all of which promote higher rates of authigenic calcite
443 precipitation.
444 An approach which is traditionally used to overcome the dilution effect is the normalization of element
445 concentrations by a conservative, lithogenic element (e.g. Kylander et al., 2011; 2013 Löwemark et al.,
446 2011; Vogel et al., 2010). In many cases, normalization allows one to identify misleading trends in
447 element concentrations. The element to be used for normalization should not itself be a proxy nor be
448 affected by biological or redox processes (Löwermark et al., 2011). Ti is widely used for normalization
449 as it is a common accessory component in various mineral phases and is conservative in terms of its
450 reactivity. However, Ti is enriched in heavy minerals and in aeolian dust, and in particular settings it can
451 therefore be used as a proxy for high-current regimes (Schnetger et al., 2000) or enhanced wind activity
452 (Wehausen and Brumsack, 1999; Yancheva et al., 2007). Another element suitable for normalization is
453 Al (Löwemark et al., 2011), which is a major component of siliciclastic mineral phases and, similar to
454 Ti, is not significantly affected by redox and biologically mediated reactions (Brumsack, 2006). Once
455 this approach is applied to our XRF series, the correlation coefficients between Zr/Al, Ti/Al and Rb/Al,
456 which are exclusively of detrital origin, remain high (Table 2, Fig. S2), and the increasing long-term
457 trend in element ratios compares well with element concentrations from ca. 129 ka to 92 ka (Fig. 6).
458 Thus, normalization using Al confirms the exclusively detrital origin for Zr, Ti and Rb, and that the
459 observed long-term trends are not an artifact caused by $CaCO_3$ dilution. Specifically, all three ratios show
460 a twofold structure, with an older (up to ca. 115 ka) part displaying a lower clastic input and a younger
461 part (90 – 115 ka) with a higher sediment delivery. They also show clear positive peaks at ca. 111 ka and
462 103 ka, corresponding to periods of higher $\delta^{18}O$ values , that we interpret as the results of drier conditions.
463 On the other hand, normalization of Si vs. Al causes correlation coefficients amongst clastic elements to
464 decrease, and highlights a decreasing Si/Al trend throughout the observed period. Because normalization
465 vs. a lithogenic element may remove the influence of mineral input to the lake (Kylander et al., 2013),
466 variations in Si/Al can be seen as reflecting the contribution of the deposition of biogenic silica. It is also
467 worth noting that correlations between Sr/Al and Si/Al and between Sr/Al and Ca/Al increase (to 0.61
468 and 0.95 respectively, Table 2), and that Sr/Al also shows a decreasing trend that mimics that of Ca and

Si, supporting the notion that part of the Sr is related to co-precipitation of Sr within the authigenic calcite as $SrCO_3$.

Now that normalization of clastic-elements vs. Al confirms the observed trends and correlations noted above, and considering the abovementioned potential causal negative relationship between calcite deposition and detrital clastic input, we can now discuss the original elemental time series in terms of paleoenvironmental changes. As a further step, in order to identify only significant and potentially climate-driven changes and to avoid overestimating variations in individual elemental concentrations using a merely visual approach, we can statistically combine Ti, Zr and Rb to produce a "clastic index" (CI hereafter) that can be compared with the stable isotope profile, assuming that all these elements respond in the same way to environmental/climatic forcings (i.e. increasing or decreasing catchment erosion). To do this, the time series of Ti, Zr and Rb were normalized to produce individual time series of anomalies (i.e., deviations from a zero mean expressed in standard deviation units, or standard scores). The standard scores of the three series were averaged to produce a CI time series where low average standard scores correspond to intervals with lower clastic input to the lake, and *vice versa*. The comparison of the CI with the $\delta^{18}O$ time series reveals a high degree of consistency (Fig. 7), for both the general patterns and short term events. Periods of reduced precipitation inferred from higher $\delta^{18}O$ values are in fact marked by increases in the CI, indicating increased catchment erosion. In particular, the drier events that are correlated with C23 and C24 North Atlantic cold events appear prominent in the CI series, whilst the events at 127.3 ka and 116.0 ka are expressed by a concomitant rise in the detrital clastic input (Fig. 7). Conversely, lower $\delta^{18}O$ values indicating wetter conditions correspond to reductions in the CI due to increase in soil-vegetation cover, and reduced flux of detrital clastics to the lake. It is worth recalling that both arid and wetter conditions may increase sediment delivery, and that temperature may have a role in vegetation development and soil erodibility. However, the good correlation between periods with higher $\delta^{18}O$ and elevated CI values supports the proposed link between drier periods and enhanced catchment erosion.

4.5.2 XRD

Due to the highly monotonous mineralogical composition of the sediments (see Section 4.2), a simple semi-quantitative approach can be applied to XRD data to test if mineralogical variations are also indicative of the same environmental changes revealed by others proxies. As previously discussed, most of the calcite is authigenic, while quartz is related to detrital input to the lake. As silicate rocks are present only marginally in the lake catchment, quartz could also have an eolian origin, as suggested for quartz-

rich loess deposits along the Apennine (Giraudi et al., 2013) and from lakes in volcanic settings from central Italy (Vico and Lagaccione Lakes; Narcisi, 2000). Plotting the ratio between peak areas of quartz and calcite (Qz/Ct) against both the CI and $\delta^{18}O$ time series (Fig. 7) the general features of the CI appear well replicated in the Qz/Ct curve, with an increasing trend throughout the interglacial and major peaks corresponding to C24 and C23 events. This similarity seems to confirm the interpretation of the XRF data, showing phases of high/low primary productivity (high/low calcite content) related to reduction/increase in the clastic input to the lake, which also supports a link between sediment mineralogy and climatic conditions. The good correspondence moreover indicates that this simple ratio can be used as a good proxy for the detrital clastic input, with the advantage to be not influenced by potential dilution effects.

4.6 Biogenic silica

Due to its resistance against post burial degradation/dissolution, bulk biogenic silica (bSi) is commonly used as a proxy to reconstruct past changes in aquatic/algal productivity (Francke et al., 2016; Prokopenko et al., 2006; Vogel et al., 2010) or changes in the delivery of dissolved silica to the lake due to variations in the rate of chemical weathering in the drainage basin (Johnson et al., 2011). In the studied interval, bSi ranges from 2.5 Wt% to 18.2 Wt% (mean 8.94, SD 3.29), (Fig. 2 and 7). It is worth noting that the two most extreme values occur in closer proximity to tephra POP2a and POP2b (Fig. 2). Tephra influx increases the silica content in the water (Barker et al. 2000) and it has been noted that such fluxes could alter lake water chemistry and benthic habitat. It could cause a shift in diatom assemblages and populations (e.g. Cvetkoska et al., 2015), and/or an increase in diatom productivity (D'Addabbo et al., 2015), and/or an increase in individual diatom frustule size (Jovanovska et al., 2016). Volcanic material is likely the primary source for Si in Sulmona. Thus, tephra deposition or mobilization from the catchment can be an important trigger for diatom blooms and increases in frustule size, largely independent of climate. With this in mind, the two samples with exceptionally high bSi concentrations centered at 102.8 ka and 102.9 ka – close to tephra deposits – can be excluded from the following discussion of climate and environmental change (Fig. 7).

Although the low resolution of the bSi curve (one sample every ~1 kyr) prevents a close comparison with the $\delta^{18}O$ time series, it is interesting to note that there is a decrease in bSi values corresponding to higher isotope values during the cold/dry event C24. Moreover, bSi decreases during the Early Last Glacial from ca. 102 ka onwards, thus mimicking the $\delta^{18}O$ trend toward higher values. The pattern during the Eemian instead is not very clear, and there is a lack of a well-expressed peak in productivity related to

full interglacial conditions. A potential explanation is related to dilution of bSi by increased calcite deposition during the LIG. This seems supported by the Si/Al curve (Fig. 6). Because normalization removes the influence of clastic Si, the highest Si/Al ratio observed during the first part of the LIG, which has no counterpart in the other clastic detrital elements (Ti, Rb, Zr), can be attributed to a higher contribution of bSi to the total Si budget related to a peak in primary productivity under full interglacial conditions.. However, higher resolution bSi analyses would be needed to test this hypothesis.

4.7 Significance of the POP record in the framework of Mediterranean climate variability during the LIG

In order to better frame the POP record in the context of regional climate variability, we can now compare it with existing regional paleoclimate archives, in an attempt to draw a coherent picture of observed variability and to unravel the potential mechanisms driving hydrological and environmental changes, for both long-term trends and short-term events.

Of particular interest is the comparison of the Sulmona $\delta^{18}O$ profile with speleothem records from Corchia Cave and Tana che Urla Cave (Fig. 8, Drysdale et al., 2007, 2009; Regattieri et al., 2012, 2014a, 2016a). These two records are both located in the western Apennines, ~400 km north of Sulmona (Fig. 1). All three oxygen isotope records show a highly coherent pattern of $\delta^{18}O$ variations with respect to timing and amplitude of the observed changes during the investigated period (Fig. 8). The fact that the precipitation signal is replicated in the three records allows us to discuss changes in $\delta^{18}O$ in terms of regional expression of the variations of the precipitation amount over the central Mediterranean area. Moreover, the comparison supports the chronology proposed for the POP record, despite the relatively high uncertainty for the lower part of the interval. By considering this good chronological and paleohydrological consistency, the onset of lake conditions in the Sulmona Basin at ca. 129 ka could be conceivably seen as the environmental response to the increase in precipitation which cause the abrupt decreasing of central Italy speleothem $\delta^{18}O$ at the Eemian onset (129.0 ± 1 ka, Drysdale et al., 2005 and 129.6 ± 1 ka, Regattieri et al. 2016a). Conversely, the peat layer at bottom of the POP lacustrine succession may be likely related to the initial stages of lake formation during the deglaciation that preceded the Eemian which follows the marked dry event centered at ca 130.5-129.5 ka documented in Tana che Urla Cave (Regattieri et al., 2014a) and recently reinterpreted as hydrological expression of the North Atlantic Heinrich event 11 (Regattieri et al. 2016a).

In all the three records, the initial part of the LIG (from ca. 129 to ca. 127 ka on the POP chronology) shows a short interval of minimum $\delta^{18}O$ values (Fig. 8). This interval suggests high precipitation and/or

565 enhanced seasonality, as discussed above. For the early part of the LIG, an enhanced Mediterranean
566 character of the precipitation (i.e., summer drought and precipitation concentrated in autumn and winter)
567 has been highlighted by several paleoclimate records (e.g. Tzedakis et al., 2003; Brauer et al., 2007;
568 Toucanne et al., 2015; Milner et al., 2012) and has been related to the northward migration of the
569 Intertropical Convergence Zone (ITCZ) during precession minima at the time of Sapropel S5 deposition
570 in the eastern Mediterranean (Milner et al., 2012; Toucanne et al., 2015). Notably, the pollen records
571 from Tenaghi Philippon (Greece, Milner et al., 2012, 2013, Fig. 8) show that the early part of the Eemian
572 corresponds to the highest percentage of Mediterranean taxa. The same applies for the pollen record from
573 the Iberian margin marine core MD95-2042 (Sanchez-Goni et al., 1999, 2007). It should be noted that
574 others pollen records from the same period, like that from Monticchio and from Ohrid lakes (Brauer et
575 al., 2007; Sadori et al., 2016), do not clearly show the same increase in Mediterranean vegetation during
576 the early Eemian. However, in both of these sites the percentage of Mediterranean essence is always low
577 (i.e. below 15%) and shows only minor variations between glacial/interglacial periods; it is thus likely
578 for these sites that variations in Mediterranean vegetation percentage are not fully representative of local
579 plant composition. The link between minimum $\delta^{18}O$ values and higher seasonality is also supported by
580 the fact that in the POP record neither the CI nor the Qz/Ct ratio show a steep increase at 127.3 ka. It
581 suggests that no abrupt and major changes in catchment erosion, related to major changes in precipitation
582 amount, happened at that time. Rather, an increase in the contribution of isotopically light winter
583 precipitation and/or a substantial reduction in isotopically enriched summer rains would have been able
584 to cause the shift of the annual weighted mean isotopic values of precipitation towards more negative
585 values (Longinelli et al., 2006), affecting $\delta^{18}O$ calcite values. This seems to be supported also by the fact
586 that the peak corresponding to GI24 in the CI series, although being well expressed, is no more prominent
587 than the previous interstadial (GI25) (Fig. 7). Conversely, in the $\delta^{18}O$ series GI24 is very pronounced, as
588 almost as the first part of the LIG (Fig. 7), and its prominence was suggested to be due to higher
589 seasonality (Regattieri et al., 2015).
590 After this short-term optimum, all three $\delta^{18}O$ records show an abrupt event of reduced precipitation
591 lasting ~1 kyr (Fig. 8), which is accompanied in the POP record by a concomitant increase in the CI (Fig.
592 7), suggesting reduction in vegetation cover and increased catchment erosion. It is interesting to note that
593 also pollen records from southern Italy (Monticchio Lake, Brauer et al., 2007), from Greece (Ioannina,
594 Tzedakis et al., 2003 and Tenaghi Philippon, Milner et al., 2013, 2016) and from the Iberian margin (core
595 MD95-2042, Sánchez Gõni et al., 1999, 2005) report a nearly coincident event of reduced arboreal pollen
596 around ca.127 ka. Thus, together these records seem to support the notion of temporarily regional climate

deterioration straight after the beginning of the LIG, although uncertainties related to each age models prevent a secure correlation.

After ca. 126 ka, the POP record shows a trend toward drier conditions and enhanced centennial-scale environmental instability until ca. 125 ka, which is well replicated in regional speleothem and pollen records (Fig. 8). Additional minor centennial-scale dry events in the POP record are centered at ca. 112.7 ka, ca. 116.0 ka and ca. 119.1 ka (Fig. 8). These events are, within chronological uncertainties, also recorded in the Corchia and Tana che Urla speleothems.

Moving to the marine realm, a high-resolution study of faunal and geochemical proxies from the western Mediterranean site ODP-975 recognized several short-term climatic events within MIS5e, which have been assigned to disruptions of the AMOC and associated changes in atmospheric circulation (Kandiano et al., 2014). Particularly, SST reconstructions from foraminifera (developed by Modern Analogue and Transfer Function techniques) show three notable cooling events centered around 122.3 ka, 119.0 ka and 114.2 ka. (Fig. 8). These events are consistent with intra-interglacial variability recognized in the western Mediterranean basin (Sprovieri et al., 2006) and mimic intra-interglacial instability emerging from North Atlantic records (McManus et al., 1994; Oppo et al., 2001, 2006; Bauch et al., 2011; Irvali et al., 2012). These decreases in SST have recently been proposed to be related to episodic cold water-mass expansions in the North Atlantic and associated southward migration of the Arctic Front (Mokeddem et al., 2014) and/or to changes in North Atlantic Deep Water (NADW) formation due to buoyance changes related to melting of persisting ice sheets (Galaasen et al., 2014). It has to be noted that the western Mediterranean faunal SST record is lacking clear evidence for the event at ca. 127 ka (Kandiano et al., 2014). However, this event falls within the deposition of an Organic Rich Layer (ORL) and corresponds to peak abundances of the cold dwelling foraminifera *Globigerinoides ruber* related to incursions of colder North Atlantic water into the Mediterranean Sea (Kandiano et al., 2014).

The influence of North Atlantic cold events on Mediterranean hydrology during the Early Last Glacial has been previously recognized in both the Sulmona and in the Corchia records (Regattieri et al., 2015; Drysdale et al., 2007). The occurrence of these events also in the POP record for the LIG thus confirms the linkage between high-latitude climate and Mediterranean hydrology under different climate boundary conditions (i.e.; glacials and interglacials), with cold/AMOC slowdown events in the North Atlantic triggering reduced precipitation in the Mediterranean. These findings also add to a growing number of paleoclimate records suggesting that large Northern Hemisphere ice sheets are not a fundamental prerequisite for triggering widespread millennial scale climate change. Instead, disruptions of the AMOC

628 that are severe enough to cause drops in SST's and associated water vapor advection and shifts in
629 atmospheric circulation patterns in the North Atlantic, during full interglacial conditions, are seemingly
630 capable of affecting the hydrology and environment of regions further downstream, such as the
631 Mediterranean.

632

633 **5. Conclusions**

634 In this work we have presented a multiproxy record ($\delta^{13}C$, $\delta^{18}O$, elemental composition, and low-
635 resolution biogenic silica and mineralogy) obtained from lacustrine sediments of the Sulmona Basin
636 (central Italy). It is anchored to an independent time-scale based on tephrochronology, here improved by
637 a new direct $^{40}Ar/^{39}Ar$ age (109.5 ± 0.9 ka, 2σ analytical uncertainty) for the widespread X-6
638 Mediterranean marker. Specifically, six tephra layers account for a relatively constant history of the
639 sediment accumulation from ca.129 ka to 92 ka, though chronological uncertainty is relatively high for
640 the older interval investigated.

641 The resulting temporal series show prominent climatic and environmental changes on both long-term
642 and millennial time-scale. . Element concentrations and sediment mineralogy (quartz / calcite ratio from
643 XRD analyses) show consistent patterns, with variations attributed to changes in the detrital clastic input
644 to the lake. Lower detrital flux indicates reduced catchment erosion due to a denser vegetation cover and
645 enhanced soil development under favorable climatic conditions, whereas enhanced mineral flux to the
646 lake is related to events of climatic/environmental deterioration. $\delta^{18}O$ values are interpreted to reflect
647 rainfall amount in the high altitude catchment of the paleo-lake, with lower values indicating enhanced
648 precipitation and possibly higher seasonality of the climate. Timing, amplitude, and general trends of the
649 observed features are in agreement between the proxies indicating stronger catchment erosion (high
650 detrital flux) during phases of lower precipitation (high $\delta^{18}O$). Our combined approach defines a clearer
651 picture of environmental evolution during the observed period and confirms the hydrological significance
652 of the $\delta^{18}O$ record from the Sulmona Basin, and more generally from the central Mediterranean
653 continental carbonates.

654 Comparison between the Sulmona $\delta^{18}O$ record and speleothem $\delta^{18}O$ records located ~400 km to the north
655 (Corchia and Tana che Urla Caves) shows consistent patterns down to the centennial time scale, and
656 highlights several intra-interglacial events of reduced precipitation, which can be correlated among the
657 three records within the associated uncertainty of each chronology. The most prominent is placed
658 between 127.3 ka and 126.3 ka. Minor events of climate deterioration (lasting ~0.5 kyr) are apparent in

659 all the continental $\delta^{18}O$ records at ca.123 ka, ca. 119 ka and ca. 116 ka, seem to have counterparts in a
660 western Mediterranean faunal SST record, and possibly correspond to episodic phases of AMOC
661 slowdown with episodic cold water-mass expansions and/or changes in the seasonal ice-sea cover in the
662 North Atlantic. Overall, the new Sulmona record shows prominent intra-interglacial variability and
663 suggests that North Atlantic SST variability during periods of low ice volume is capable of disrupting
664 water vapor advection and atmospheric circulation patterns that feed Mediterranean hydrology.

665

666 **Acknowledgments**

667 This work was funded by the Australian Research Council Discovery Project DP160102969and by the
668 University of Pisa through the project P.R.A. 2016 "*Ruolo di zone di taglio nella costruzione degli*
669 *orogeni: case histories da catene orogenetiche*". ER is supported by project SFB806 "Our way to
670 Europe". G. Zanchetta is thanked for discussion and comments to an early version of the manuscript. L.
671 Folco is thanked for access to the HHXRF units, funded by the Italian "Ministero degli Affari Esteri"
672 (project ID#: PGR00187). D. Pecci, G. Luceretti and C. Gini are thanked for XRD data collection and
673 R. Anis Ishak Nakhla is thanked for FESEM investigations. Two anonymous reviewer are also thanked
674 for useful comments on the first version of the manuscript.

675

676 **References**

677 Alpert, P., Baldi, M., Ilani, R., Krichak, S., Price, C., Rodo, X., Xoplaki, E., 2006. Relations between
678 climate variability in the Mediterranean region and the tropics: ENSO, South Asian and African
679 monsoons, hurricanes and Saharan dust. Developments in Earth and Environmental Sciences 4, 149-177.

680 Barbieri, M., Boschetti, T., Petitta, M., Tallini, M. 2005. Stable isotope (^{2}H, ^{18}O and $^{87}Sr/^{86}Sr$) and
681 hydrochemistry monitoring for ground water hydrodinamics analyses in a karst aquifer (Gran Sasso,
682 Central Italy). Applied Geochemistry 20, 2063-2081.

683 Bard, E., Delaygue, G., Rostek, F., Antonioli, F., Silenzi, S., Schrag, D. 2002. Hydrological conditions
684 in the western Mediterranean basin during the deposition of Sapropel 6 (ca. 175 kyr). Earth Planetary
685 Sciences Letters 202, 481-494.

686 Barker, P., Telford, R., Merdaci, O., Williamson, D., Taieb, M., Vincens, A., Gibert, E. 2000. The
687 sensitivity of a Tanzanian crater lake to catastrophic tephra input and four millennia of climate change.
688 The Holocene, 10(3), 303-310.

689 Bar-Matthews, M., Ayalon, A., Kaufmann, A., 2000. Timing and hydrological conditions of sapropel
690 events in the eastern Mediterranean, as evident from speleothems, Soreq Cave, Israel. Chemical Geology
691 169, 145–156.

692 Bar-Matthews, M., Ayalon, A., Gilmor, M., Matthews, A., Hawkeshworth, C.J., 2003. Sea–land oxygen
693 isotopic relationships from planktonic foraminifera and speleothems in the Eastern Mediterranean region
694 and their implication for paleorainfall during interglacial intervals. Geochimica et Cosmochimica Acta
695 67, 3181–3199.

696 Bauch, H.A., Kandiano, E.S., Helmke, J.P. 2012. Contrasting ocean changes between the subpolar and
697 polar North Atlantic during the past 135 ka. Geophysical Research Letters, 39(11).

698 Berger, A., Loutre, M. F. 1991. Insolation values for the climate of the last 10 million years. Quaternary
699 Science Reviews 10(4), 297-317.

700 Blaauw, M. 2010. Methods and code for 'classical'age-modelling of radiocarbon sequences. quaternary
701 geochronology 5(5), 512-518.

702 Boch, R., Cheng, H., Spötl, C., Edwards, R.L., Wang, X. 2011. NALPS: a precisely dated European
703 climate record 120-60 ka. Climate of the Past 7(4), 1247-1259.

704 Bourne, A.J., Albert, P.G., Matthews, I.P., Trincardi, F., Wulf, S., Asioli, A., Blockley, S.P., Keller, J., Lowe J.J.
705 2015. Tephrochronology of core PRAD 1–2 in the Adriatic Sea: insights into Italian explosive volcanism for the
706 period 200–80 ka. Quaternary Science Reviews 16, 28–43.

707 Brauer A., Allen J.R.M., Mingram J., Dulski P., Wulf, S., Huntley, B., 2007. Evidence for the last
708 interglacial chronology and environmental change from Southern Europe. Proceeding of the National
709 Academy of Science USA 104, 450-455.

710 Brumsack, H.-J. 2006. The trace metal content of recent organic carbon-rich sediments: implications for
711 Cretaceous black shale formation. Palaeogeography, Palaeoclimatology, Palaeoecology 232 (2–4), 344–
712 361.

713 Cacho, I., Grimalt, J.O., Sierro, F.J., Shackleton, N.J., Canals, M., 2000. Evidence of enhanced
714 Mediterranean thermohaline circulation during the rapid climatic coolings. Earth Planetary Science
715 Letters 183, 417-429.

716 Cavinato G.P., Cosentino, D., De Rita, D., Funiciello, R., Parotto M. 1994. Tectonicsedimentary
717 evolution of intrapenninic basins and correlation with the volcano-tectonic activity in central Italy.
718 Memorie Descrittive della Carta Geologica d'Italia 49, 63–76.

719 Cavinato, G.P., Miccadei, E. 1995. Sintesi preliminare delle caratteristiche tettoniche e sedimentarie dei
720 depositi quaternari della conca di Sulmona (L'Aquila). Journal of Quaternary Science 8, 129–140.

721 Cavinato, G.P, Miccadei, E. 2000. Pleistocene carbonate lacustrine deposits: Sulmona basin (central
722 Apennines, Italy). In Lake Basins Through Space and Time. Gierlowsky-Kordesch EH, Kelts KR (eds.).
723 Studies in Geology, American Association of Petroleum Geologists 46, 517–526.

724 Celle-Jeanton, H., Travi, Y., Blavoux, B. 2001. Isotopic typology of the precipitation in the Western
725 Mediterranean region at three different time scales. Geophysical Research Letters 28, 1215-1218.

726 Couchoud, I., Genty, D., Hoffmann, D., Drysdale, R.N., Blamart, D. 2009. Millennial-scale variability
727 during the Last Interglacial recorded in a speleothem from south-western France. Quaternary Science
728 Reviews 28, 3263-3274.

729 Curry, W. B., Oppo, D. W., 1997. Synchronous, high-frequency oscillations in tropical sea surface
730 temperatures and North Atlantic Deep Water production during the last glacial cycle. Paleoceanography,
731 12, 1-14.

732 Cvetkoska, A., Levkov, Z., Reed, J.M., Wagner, B., Panagiotopoulos, K., Leng, M.J., Lacey, J.H. 2015.
733 Quaternary climate change and Heinrich events in the southern Balkans: Lake Prespa diatom
734 palaeolimnology from the last interglacial to present. Journal of Paleolimnology 53(2), 215-231.

735 D'Addabbo, M., Sulpizio, R., Guidi, M., Capitani, G., Mantecca, P., Zanchetta, G. Ash leachates from
736 some recent eruptions of Mount Etna (Italy) and Popocatépetl (Mexico) volcanoes and their impact on
737 amphibian living freshwater organisms, Biogeosciences 12, 7087–7106.

738 Desiderio, G., Rusi, S., Tatangelo, F. 2005a: Utilizzo di tecniche isotopiche (^{18}O e ^{2}H) nello studio delle
739 acque sotterranee in aree protette dell'Appennino Abruzzese. Rivista italiana di Agrometeorologia 9/1,
740 90-91.

741 Desiderio, G., Ferracuti, L., Rusi, S., Tatangelo, F. 2005b. Il contributo degli isotopi naturali ^{18}O e ^{2}H
742 nello studio delle idrostrutture carbonatiche abruzzesi e delle acque mineralizzate nell'area abruzzese e
743 molisana. Giornale di Geologia Applicata 2, 453-458.

744 Donato, P., Albert, P.G., Crocitti, M., De Rosa, R., Menzies, M.A. 2016. Tephra layers along the southern
745 Tyrrhenian coast of Italy: Links to the X-5 & X-6 using volcanic glass geochemistry. Journal of
746 Volcanology and Geothermal Research 317, 30-41.

747 Drysdale, R.N., Zanchetta, G., Hellstrom, J.C., Fallick, A.E., Zhao, J.X., Isola, I., Bruschi, G. 2004.
748 Palaeoclimatic implications of the growth history and stable isotope ($\delta^{18}O$ and $\delta^{13}C$) geochemistry of a
749 Middle to Late Pleistocene stalagmite from central western Italy. Earth and Planetary Science Letters
750 227, 215–229.

751 Drysdale, R.N, Zanchetta, G., Hellstrom, J.C., Fallick, A.E., Zhao, J.X. 2005. Stalagmite evidence for
752 the onset of the Last Interglacial in southern Europe at 129 ± 1 ka. Geophysical Research Letters 32,

753 Drysdale, R.N., Zanchetta, G., Hellstrom, J.C., Maas, R., Fallick, A.E., Pickett, M., Cartwright, I.,
754 Piccini, L., 2006. Late Holocene drought responsible for the collapse of Old World civilizations is
755 recorded in an Italian cave flowstone. Geology 34, 101-104.

756 Drysdale, R.N., Zanchetta, G., Hellstrom, J.C., Fallick, A.E., McDonald, J., Cartwright, I. 2007.
757 Stalagmite evidence for the precise timing of North Atlantic cold events during the early last glacial.
758 Geology 35, 77-80.

759 Drysdale, R.N., Hellstrom, J.C., Zanchetta, G., Fallick, A.E., Sánchez Goñi, M.F., Couchoud, I.,
760 McDonald J., Maas, R., Lohmann, G., Isola, I. 2009. Evidence for Obliquity Forcing of Glacial
761 Termination II. Science 325, 1527-1531.

762 Eshel, G., 2002. Mediterranean climates. Israel Journal of Earth Sciences 51, 157-168.

763 Falcone, R.A, Falgiani, A., Parisse, B., Petitta, M., Spizzico, M., Tallini M. 2008. Chemical and isotopic
764 ($\delta^{18}O‰$, $\delta^{2}H‰$, $\delta^{13}C‰$, ^{222}Rn) multi-tracing for groundwater conceptual model of carbonate aquifer
765 (Gran Sasso INFN underground laboratory-central Italy). Journal of Hydrology 357, 368-388.

766 Francke, A., Wagner, B., Just, J., Leicher, N., Gromig, R., Baumgarten, H., Vogel, H., Lacey, J.H.,
767 Sadori, L., Wonik T., Leng, M.J. Zanchetta G., Sulpizio, R., Giaccio, B., 2016. Sedimentological
768 processes and environmental variability at Lake Ohrid (Macedonia, Albania) between 637 ka and the
769 present. Biogeosciences 13(4), 1179-1196.

770 Freytet, P., Verrecchia, E.P. 2002. Lacustrine and palustrine carbonate petrography: an overview. Journal
771 of Paleolimnology 27(2), 221-237.

772 Galaasen, E.V., Ninnemann, U.S., Irvalı, N., Kleiven, H.K.F., Rosenthal, Y., Kissel, C., Hodell, D.A.
773 2014. Rapid reductions in North Atlantic Deep Water during the peak of the last interglacial period.
774 Science 343(6175), 1129-1132.

775 Gemelli, M., D'Orazio, M., Folco, L. 2015. Chemical Analysis of Iron Meteorites Using a Hand-Held X-
776 Ray Fluorescence Spectrometer. Geostandards and Geoanalytical Research 39(1), 55-69.

777 Galli, P., Giaccio, B., Peronace, E., Messina, P., 2015. Holocene paleoearthquakes and Early-Late
778 Pleistocene slip-rate on the Sulmona Fault (Central Apeninnes, Italy). Bulletin of the Seismological
779 Society of America 105, 1–13.

780 Giaccio, B., Messina, P., Sposato, A., Voltaggio, M., Zanchetta, G., Galadini, F., Gori, S., Santacroce,
781 R. 2009. Tephra layers from Holocene lake sediments of the Sulmona Basin, central Italy: implications
782 for volcanic activity in Peninsular Italy and tephrostratigraphy in the central Mediterranean area.
783 Quaternary Science Reviews 28(25), 2710-2733.

784 Giaccio, B., Nomade, N., Wulf, S., Isaia, R., Sottili, G., Cavuoto, G., Galli, P., Messina, P., Sposato, A.,
785 Sulpizio, R., Zanchetta, G. 2012. The late MIS 5 Mediterranean tephra markers: a reappraisal from
786 peninsular Italy terrestrial records. Quaternary Science Reviews 56, 31-45.

787 Giaccio, B., Castorina, F., Nomade, S., Scardia, G., Voltaggio, M., Sagnotti. L. 2013a. Revised
788 chronology of the Sulmona lacustrine succession, central Italy. Journal of Quaternary Science 28, 545–
789 551.

790 Giaccio, B., Arienzo, I., Sottili, G., Castorina, F., Gaeta, M., Nomade, S., Galli, P., Messina, P. 2013b.
791 Isotopic (Sr-Nd) and major element fingerprinting of distal tephras: an application to the Middle-Late
792 Pleistocene markers from the Colli Albani volcano, central Italy. Quaternary Science Reviews 67, 190-
793 206.

794 Giaccio, B., Regattieri, E., Zanchetta, G., Nomade, S., Renne, P.R., Sprain, C.J., Drysdale, R.N.,
795 Tzedakis, P.C., Messina, P., Scardia, G., Sposato, A., Bassinot, F. 2015a. Duration and dynamics of the
796 best orbital analogue to the present interglacial. Geology 43 (7), 603-606.

797 Giaccio, B., Regattieri, E., Zanchetta, G., Wagner, B., Galli, P., Mannella, G., Niespolo, E., Peronace,
798 E., Renne, P., Nomade, S., Cavinato, G.P., Messina, P., Sposato, A., Boschi, C., Florindo, F., Marra, F.,
799 Sadori L. 2015b. A key continental archive for the last 2 Ma of climatic history in central Mediterranean
800 area: a preliminary report on the Fucino deep-drilling project, central Italy. Scientific Drilling 3, 1–7.

801 Gierlowsky-Kordesch, E.H. 2010. Lacustrine carbonates. In Developments in Sedimentology 61, 2-50.

802 Insinga, D.D., Tamburrino, S., Lirer, F., Vezzoli, L., Barra, M., De Lange, G.J., Tiepolo, M., Vallefuoco,
803 M., Mazzola, S., Sprovieri, M. 2014. Tephrochronology of the astronomically-tuned KC01B deep-sea
804 core, Ionian Sea: Insights into the explosive activity of the Central Mediterranean area during the last
805 200 ka. Quaternary Science Reviews 85, 63-84.

806 Giraudi, C., Magny, M., Zanchetta, G., Drysdale, R.N., 2011. The Holocene climatic evolution of the
807 Mediterranean Italy: a review of the geological continental data. The Holocene 21, 105-115.

808 Giraudi, C., Zanchetta, G., Sulpizio, R. (2013). A Late-Pleistocene phase of Saharian dust deposition in
809 the high Apennine mountains (Italy). Alpine Mediterranean Quaternary, 26, 110-122.

810 Govin, A., Capron, E., Tzedakis, P. C., Verheyden, S., Ghaleb, B., Hillaire-Marcel, C., St-Onge, G.,
811 Stoner, J.S., Bassinot, F., Bazin, L., Blunier, T., N. Combourieu-Nebout, N., El Ouahabi, A., Genty, D.,
812 Gersonde, R., Jimenez-Amat, P., A. Landais, A., Martrat, B., Masson-Delmotte, V., Parrenin F.,
813 Seidenkrantz M.S., Veres D., Waelbroeck C., Zahn R. 2015. Sequence of events from the onset to the

814 demise of the Last Interglacial: Evaluating strengths and limitations of chronologies used in climatic
815 archives. Quaternary Science Reviews, 129, 1-36.

816 Hollander, D.J., McKenzie, J.A. 1991. CO_2 control on carbon-isotope fractionation during aqueous
817 photosynthesis: a paleo-pCO_2 barometer. Geology 19, 929–932.

818 Iorio, M., Liddicoat, J., Budillon, F., Incoronato, A., Coe, R.S., , Insinga, D., Cassata, W., Lubritto, C.,
819 Angelino, A., Tamburrino, S.. 2014.Combined palaeomagnetic secular variation and petrophysical
820 records to time constrain geological and hazardous events: an example from the eastern Tyrrhenian Sea
821 over the last 120 ka. Global and Planetary Changes 113, 91-109.

822 Irvali, N., Ninnemann, U.S., Galaasen, E.V., Rosenthal, Y., Kroon, D., Oppo, D.W., Kleiven, H.F.,
823 Darling, K.F., Kissel, C. 2012. Rapid switches in subpolar North Atlantic hydrography and climate
824 during the Last Interglacial (MIS 5e). Paleoceanography 27 (2), PA2207

825 Johnson, T. C., Brown, E. T., Shi, J. 2011. Biogenic silica deposition in Lake Malawi, East Africa over
826 the past 150,000 years. Palaeogeography, Palaeoclimatology, Palaeoecology 303(1), 103-109.

827 Jovanovska, E., Cvetkoska, A., Hauffe, T., Levkov, Z., Wagner, B., Sulpizio, R., Francke, A., Albrecht,
828 C., Wilke, T. 2016. Differential resilience of ancient sister lakes Ohrid and Prespa to environmental
829 disturbances during the Late Pleistocene. Biogeosciences 13(4), 1149-1161.

830 Kandiano, E.S., Bauch, H.A., Fahl, K. 2014. Last interglacial surface water structure in the western
831 Mediterranean (Balearic) Sea: Climatic variability and link between low and high latitudes. Global and
832 Planetary Change 123, 67-76.

833 Keller, J., Ryan, W.B.F., Ninkovich, D., Altherr, R. 1978. Explosive volcanic activity in the
834 Mediterranean over the past 200,000 years as recorded in deep-sea sediments. Geological Society of
835 America Bulletin 89, 591-604.

836 Kelts, K., Hsü, K.J. 1978. Freshwater carbonate sedimentation. In Lakes, Chemistry, Geology, Physics,
837 (ed.). Lerman A Springer-Verlag: Berlin, 295–323.

838 Kelts, K., Talbot, M. 1990. Lacustrine carbonates as geochemical archives of environmental change and
839 biotic/abiotic interactions. In Large Lakes (pp. 288-315). Springer Berlin Heidelberg.

840 Kim, S.T., O'Neil, J.R. 1997. Equilibrium and nonequilibrium oxygen isotope effects in synthetic
841 carbonates. Geochimica et Cosmochimica Acta, 61(16), 3461-3475.

842 Koinig, K.A., Shotyk, W., Lotter, A.F., Ohlendorf, C., Sturm, M. 2003. 9000 years of geochemical
843 evolution of lithogenic major and trace elements in the sediment of an alpine lake – the role of climate,
844 vegetation and land-use history. Journal of Paleolimnology 30, 307–320.

845 Kylander, M.E., Ampel, L., Wohlfarth, B., Veres, D., 2011. High-resolution X-ray fluorescence core
846 scanning analysis of Les Echets (France) sedimentary sequence: new insights from chemical proxies.
847 Journal of Quaternary Sciences 26 (1), 109-117.

848 Kylander, M.E., Klaminder, J., Wohlfarth, B., Löwemark, L. 2013. Geochemical responses to
849 paleoclimatic changes in southern Sweden since the late glacial: the Hässeldala Port lake sediment
850 record. Journal of Paleolimnology 50(1), 57-70.

851 Kukla, G. J., Bender, M. L., de Beaulieu, J. L., Bond, G., Broecker, W. S., Cleveringa, P., Gavin J.E.,
852 Herbert T.D., Imbrie J., Jouzel J., Keigwin, L. D., Knudsen K-L., McManus J., Merkt J., Muhs D.R.,
853 Muller H., Poore R.Z., Porter S.C. 2002. Last Interglacial Climates. Quaternary Research 58(1), 2-13.

854 Leicher, N., Zanchetta, G., Sulpizio, R., Giaccio, B., Wagner, B., Nomade, S., Francke, A., Del Carlo, P.
855 2016 First tephrostratigraphic results of the DEEP site record from Lake Ohrid (Macedonia and Albania).
856 Biogeosciences, 13, 2151–2178.

857 Leng, M.J., Marshall, J.D. 2004. Palaeoclimate interpretation of stable isotope data from lake sediment
858 archives. Quaternary Science Reviews 23, 811–831.

859 Leng, M. J., Jones, M. D., Frogley, M. R., Eastwood, W. J., Kendrick, C. P., Roberts, C. N. 2010. Detrital
860 carbonate influences on bulk oxygen and carbon isotope composition of lacustrine sediments from the
861 Mediterranean. Global and Planetary Change, 71(3), 175-182.

862 Lézine, A.M., von Grafenstein, U., Andersen, N., Belmecheri, S., Bordon, A., Caron, B., Cazet, P.,
863 Erlenkeuser, H., Fouache, E., Grenier, C., Huntsman-Mapila, P., Hureau-Mazaudier, D., Manelli, D.,
864 Mazaud, A., Robert, C., Sulpizio, R., Tiercelin, J.J., Zanchetta, G., Zeqollari, Z. 2010. Lake Ohrid,
865 Albania, provides an exceptional multi-proxy record of environmental changes during the last glacial-
866 interglacial cycle. Palaeogeography, Palaeoclimatology, Palaeoecology 287, 116–127.

867 Lionello, P., Bhend, J., Buzzi, A., Della-Marta, P.M., Krichak, S., Jansà, A., Maheras, P., Sanna, A.,
868 Trigo, I.F., Trigo, R. 2006. Cyclones in the Mediterranean region: climatology and effects on the
869 environment. In P. Lionello, P. Malanotte-Rizzoli, R. Boscolo (eds) Mediterranean Climate Variability.
870 Amsterdam: Elsevier (NETHERLANDS), 324-272.

871 Longinelli, A., Selmo, E., 2003. Isotopic composition of precipitation in Italy: a first overall map. Journal
872 of Hydrology 270, 75-88.

873 Longinelli, A., Anglesio, E., Flora, O., Iacumin, P., Selmo, E. 2006. Isotopic composition of precipitation
874 in Northern Italy: reverse effect of anomalous climatic events. Journal of Hydrology 329(3), 471-476.

875 Lowe, D. J. 2011. Tephrochronology and its application: a review. Quaternary Geochronology 6(2), 107-
876 153.

877 Löwemark, L., Chen, H.F., Yang, T.N, Kylander, M.E., Yu, E.F., Hsu, Y.W., Lee, T.Q., Song, S.R.,
878 Jarvis, S. 2011. Normalizing XRF-scanner data: a cautionary note on the interpretation of high-resolution
879 records from organic-rich lakes. Journal of Asian Earth Sciences 40,1250–1256

880 Mayer, B., Schwark, L. 1999. A 15,000-year stable isotope record from sediments of Lake Steisslingen,
881 Southwest Germany. Chemical Geology 161, 315–337.

882 Marino, G., Rohling, E.J., Rodríguez-Sanz, L., Grant, K.M., Heslop, D., Roberts, A.P., Stanford, J.D.,
883 Yu, J., 2015. Bipolar seesaw control on last interglacial sea level. Nature 522 (7555), 197-201.

884 Martrat, B., Grimalt, J.O., Lopez-Martinez, C., Chaco, I., Sierro, F.J., Flores, J.A., Zahn, R., Canals, M.,
885 Jason, H.C., Hodell, D.A., 2004. Abrupt temperature changes in the Western Mediterranean over the past
886 250,000 years. Science 306, 1762–1765.

887 Martrat, B., Jimenez-Amat, P., Zahn, R., & Grimalt, J. O. 2014. Similarities and dissimilarities between
888 the last two deglaciations and interglaciations in the North Atlantic region. Quaternary Science Reviews
889 99, 122-134.

890 Meyer-Jacob, C., Vogel, H., Boxberg, F., Rosén, P., Weber, M.E., and Bindler, R. 2014. Independent
891 measurement of biogenic silica in sediments by FTIR spectroscopy and PLS regression. Journal of
892 Paleolimnology 52, 245-255.

McManus, J., Bond, G., Broecker, W., Johnsen, S., Labeyrie, L., Higgins, S., 1994. High-resolution climate records from the North Atlantic during the Last Interglacial. Nature 371, 326–329.

Miccadei, E., Barberi, R., Cavinato, G.P. 1998. La geologia quaternaria della conca di Sulmona (Abruzzo, Italia centrale). Geologica Romana 34, 59–86.

Milner, A. M., Collier, R. E., Roucoux, K. H., Müller, U. C., Pross, J., Kalaitzidis, S., Tzedakis, P. C., 2012. Enhanced seasonality of precipitation in the Mediterranean during the early part of the Last Interglacial. Geology 40, 919-922.

Milner, A. M., Müller, U. C., Roucoux, K. H., Collier, R. E., Pross, J., Kalaitzidis, S., Tzedakis, P. C. 2013. Environmental variability during the Last Interglacial: a new high-resolution pollen record from Tenaghi Philippon, Greece. Journal of Quaternary Science 28(2), 113-117.

Milner, A. M., Roucoux, K. H., Collier, R. E. L., Müller, U. C., Pross, J., Tzedakis, P. C. 2016. Vegetation responses to abrupt climatic changes during the Last Interglacial Complex (Marine Isotope Stage 5) at Tenaghi Philippon, NE Greece. Quaternary Science Reviews, 154, 169-181.

Mook, W.G., Tan, F.C. 1991. Stable carbon isotopes in rivers and estuaries. In: Biogeochemistry of Major World Rivers, Degens ET, Kempe S, Richey E (eds). John Wiley: New York; 245–264.

Narcisi, B. 2000. Late Quaternary eolian deposition in central Italy. Quaternary Research, 54(2), 246-252.

North Greenland Ice Core Project Members, 2004, High-resolution record of Northern Hemisphere climate extending into the last interglacial period. Nature 431, 147–151.

Nomade, S., Renne, P.R., Vogel, N., Deino, A.L., Sharp, W.D., Becker, T.A., Jaouni, A.R., Mundil, R., 2005. Alder Creek sanidine (ACs-2): a Quaternary $^{40}Ar/^{39}Ar$ dating standard tied to the Cobb Mountain geomagnetic event. Chemical Geology 218, 315-338.

Nomade, S., Gauthier, A., Guillou, H., Pastre, J.F., 2010. $^{40}Ar/^{39}Ar$ temporal framework for the Alleret maar lacustrine sequence (French Massif-Central): volcanological and paleoclimatic implications. Quaternary Geochronology 5, 20-27.

Oehlerich, M., Baumer, M., Lücke, A., Mayr, C. 2013. Effects of organic matter on carbonate stable isotope ratios ($\delta^{13}C$, $\delta^{18}O$ values)–implications for analyses of bulk sediments. Rapid Communications in Mass Spectrometry 27, 707-712.

Oppo, D.W., Keigwin, L.D., McManus, J.F. 2001. Persistent suborbital climate variability in marine isotope stage 5 and Termination II. Paleoceanography 16, 280–292.

Oppo, D.W., McManus, J.F., Cullen, J.L. 2006. Evolution and demise of the Last Interglacial warmth in the subpolar North Atlantic. Quaternary Science Reviews 25, 3268–3277.

Paterne, M., Guichard, F., Duplessy, J.C., Siani, G., Sulpizio, R., Labeyrie, J. 2008. A 90,000-200,000 years marine tephra record of Italian volcanic activity in the Central Mediterranean Sea. Journal of Volcanology and Geothermal Research 177, 187-196.

Petrosino, P., Morabito, S., Jicha, B. R., Milia, A., Sprovieri, M., Tamburrino, S. 2016. Multidisciplinary tephrochronological correlation of marker events in the eastern Tyrrhenian Sea between 48 and 105ka. Journal of Volcanology and Geothermal Research 315, 79-99.

Pol, K., Masson-Delmotte, V., Cattani, O., Debret, M., Falourd, S., Jouzel, J., Landais A., Minster B., Mudelsee M., Schulz M., Stenni, B. 2014. Climate variability features of the last interglacial in the East Antarctic EPICA Dome C ice core. Geophysical Research Letters 41(11), 4004-4012.

Prokopenko, A.A., Hinnov, L.A., Williams, D.F., Kuzmin, M.I., 2006. Orbital forcing of continental climate during the Pleistocene: a complete astronomically tuned climatic record from Lake Baikal, SE Siberia. Quaternary Science Reviews 25, 3431–3457.

R Development Core Team, 2010. R: A Language and Environment for Statistical Computing. R Foundation for Statistical Computing, Vienna, Austria, ISBN 3-900051-07-0.

Rasmussen, T. L., Thomsen, E., Labeyrie, L., & van Weering, T. C.,1996. Circulation changes in the Faeroe-Shetland Channel correlating with cold events during the last glacial period (58–10 ka). Geology 24, 937-940.

942 Regattieri E., Isola I., Zanchetta G., Drysdale R.N., Hellstrom J.C., Baneschi I. 2012 -Stratigraphy,
943 petrography and chronology of speleothem concretion at Tana Che Urla (Lucca, Italy): paleoclimatic
944 implications. Geografia Fisica e Dinamica del Quaternario, 35, 141-152

945 Regattieri E., Zanchetta G., Drysdale R.N., Isola I., Roncioni A. 2014a. A continuous stable isotopic
946 record from the Penultimate glacial maximum to the Last Interglacial (159 to 121 ka) from Tana Che
947 Urla Cave (Apuan Alps, central Italy). Quaternary Research 82, 450–461.

948 Regattieri E., Zanchetta G., Drysdale R., Isola I., Hellstrom J., Dallai, L. 2014b. Lateglacial to Holocene
949 trace element record (Ba, Mg, Sr) from Corchia Cave (Apuan Alps, central Italy): paleoenvironmental
950 implications. Journal of Quaternary Science, 29(4), 381-392.

951 Regattieri E., Giaccio B., Zanchetta G., Drysdale R.N., Galli P., Nomade S., Peronace E., Wulf S. 2015.
952 Hydrological variability over the Apennines during the Early Last Glacial precession minimum, as
953 revealed by a stable isotope record from Sulmona basin, Central Italy. Journal of Quaternary Science
954 30(1), 19-31.

955 Regattieri E., Zanchetta G., Drysdale R.N., J.D.Woodhead, Hellstrom J., Giaccio B., Isola I., Greig A.,
956 Baneschi. 2016a. Environmental variability between the penultimate deglaciation and the mid Eemian:
957 insights from Tana che Urla (central Italy) speleothem trace element record". Quaternary Science
958 Reviews 152, 80-92.

959 Regattieri, E., Giaccio, B., Galli, P., Nomade, S., Peronace, E., Messina P., Sposato, A., Boschi, C.,
960 Gemelli, M. 2016b. A multi-proxy record of MIS 11-12 deglaciation and glacial MIS 12 instability from
961 the Sulmona Basin (central Italy). Quaternary Science Reviews, 32, 129-145.

962 Roberts, N., Jones, M.D., Benkaddur, A., Eastwood, W.J., Filippi, M.L., Frogley, M.R., Lamb, H.F.,
963 Leng, M.J., Reed, J.M., Stein, M., Stevens, L., Valero- Garcè, B., Zanchetta, G., 2008. Stable isotope
964 records of Late Quaternary climate and hydrology from Mediterranean lakes: the ISOMED synthesis.
965 Quaternary Science Review 27, 2426-2441.

966 Rohling, E.J., Marino, G., Grant, K.M., 2015. Mediterranean climate and oceanography, and the periodic
967 development of anoxic events (sapropels). Earth Science Reviews 143, 62-97.

968 Rosén, P., Vogel, H., Cunningham, L., Reuss, N., Conley, D. J., Persson, P. 2010. Fourier transform
969 infrared spectroscopy, a new method for rapid determination of total organic and inorganic carbon and
970 biogenic silica concentration in lake sediments. Journal of Paleolimnology, 43(2), 247-259.

971 Russo-Ermolli, E., Aucelli, P.P., Di Rollo, A., Mattei, M., Petrosino, P., Porreca, M., Rosskopf, C.M.,
972 2010. An integrated stratigraphical approach to the Middle Pleistocene succession of the Sessano basin
973 (Molise, Italy). Quaternary International 225 (1), 114-127.

974 Sadori, L., Koutsodendris, A., Masi, A., Bertini, A., Combourieu-Nebout, N., Francke, A., Kouli, K.,
975 Joannin, S., Mercuri, A.M., Peyron, O., Torri P., Wagner, B., Zanchetta, G., Sinopoli, G., Donders, T.H.
976 2016. Pollen-based paleoenvironmental and paleoclimatic change at Lake Ohrid (SE Europe) during the
977 past 500 ka. Biogeosciences, 13, 1423–1437.

978 Sagnotti, L., Scardia, G., Giaccio, B., Liddicoat, J.C., Nomade, S., Renne, P.R., Sprain, C.J. 2014.
979 Extremely rapid directional change during Matuyama-Brunhes geomagnetic polarity reversal.
980 Geophysical Journal International 199, 1110–1124.

981 Sagnotti, L., Giaccio, B., Liddicoat, J. C., Nomade, S., Renne, P. R., Scardia, G., & Sprain, C. J. (2016).
982 How fast was the Matuyama–Brunhes geomagnetic reversal? A new subcentennial record from the
983 Sulmona Basin, central Italy. Geophysical Journal International 204(2), 798-812.

984 Sáñchez-Goñi, M.F., Eynaud, F., Turon, J. L., Shackleton, N. J. 1999. High resolution palynological
985 record off the Iberian margin: direct land-sea correlation for the Last Interglacial complex. Earth and
986 Planetary Science Letters 171(1), 123-137.

987 Schnetger, B., Brumsack, H.J., Schale, H., Hinrichs, J., Dittert, L., 2000. Geochemical characteristics of
988 deep-sea sediments from the Arabian Sea: a high-resolution study. Deep Sea Research Part II 47, 2735–
989 2768

990 Scholz, D., Hoffmann, D.L. 2011. StalAge – An algorithm designed for construction of speleothem age
991 models. Quaternary Geochronology 6, 369–382.

992 Sirocko, F., Seelos, K., Schaber, K., Rein, B., Dreher, F., Diehl, M., Lehne, R., Jäger, K., Krbetschek,
993 M., Degering, D. 2005. A late Eemian aridity pulse in central Europe during the last glacial inception.
994 Nature 436, 833–836.

995 Seelos, K., Sirocko, F. 2007. Abrupt Cooling Events at the Very End of the Last Interglacial. The climate
996 of the past interglacial. Development in Quaternary Sciences 7, 207-229

997 Seelos, K., Sirocko, F., Dietrich, S. 2009. A continuous high-resolution dust record for the reconstruction
998 of wind systems in central Europe (Eifel, Western Germany) over the past 133 ka. Geophysical Research
999 Letters 36(20).

1000 Sprovieri, R., Di Stefano, E., Incarbona, A., Oppo, D. W. (2006). Suborbital climate variability during
1001 Marine Isotopic Stage 5 in the central Mediterranean basin: evidence from calcareous plankton record.
1002 Quaternary Science Reviews, 25(17), 2332-2342.

1003 Sulpizio, R., Zanchetta, G., D'Orazio, M., Vogel, H., Wagner, B. 2010. Tephrostratigraphy and
1004 tephrochronology of lakes Ohrid and Prespa, Balkans. Biogeosciences 7, 3273-3288.

1005 Talbot M.R. 1990. A review of the palaeohydrological interpretation of carbon and oxygen isotopic ratios
1006 in primary lacustrine carbonates. Chemical Geology: Isotope Geoscience Section 80(4), 261-279.

1007 Toucanne, S., Minto'o, C. M. A., Fontanier, C., Bassetti, M. A., Jorry, S. J., Jouet, G. 2015. Tracking
1008 rainfall in the northern Mediterranean borderlands during sapropel deposition. Quaternary Science
1009 Reviews 129, 178-195.

1010 Tzedakis, P. C., Frogley, M. R., & Heaton, T. H. E. 2003. Last Interglacial conditions in southern Europe:
1011 evidence from Ioannina, northwest Greece. Global and Planetary Change 36(3), 157-170.

1012 Tzedakis, P.C., 2007. Seven ambiguities in the Mediterranean palaeoenvironmental narrative."
1013 Quaternary Science Reviews 26, 2042-2066.

1014 Vidal, L., Labeyrie, L., Cortijo, E., Arnold, M., Duplessy, J. C., Michel, E., Van Weering, T. C. E., 1997.
1015 Evidence for changes in the North Atlantic Deep Water linked to meltwater surges during the Heinrich
1016 events. Earth and Planetary Science Letters 146, 13-27.

1017 Villa V., Pereira A., Chaussé C., Nomade S., Giaccio B., Limondin-Lozouet N., Fusco F., Regattieri E.,
1018 Degeai J.P., Robert V., Kuzucuoglu C., Boschian G., Aureli; D., Pagli M., Bahain J.J., Nicoud E. A MIS
1019 15-MIS 12 record of environmental changes and Lower Palaeolithic occupation from Valle Giumentina,
1020 central Italy. Quaternary Science Reviews 151, 160-184

1021 Vogel, H., Rosén, P., Wagner, B., Melles, M., Persson, P. 2008. Fourier transform infrared spectroscopy,
1022 a new cost-effective tool for quantitative analysis of biogeochemical properties in long sediment records.
1023 Journal of Paleolimnology 40(2), 689-702.

1024 Vogel, H., Wagner, B., Zanchetta, G., Sulpizio, R., Rosén, P. 2010. A paleoclimatic record with
1025 tephrochronological age control for the last glacial-interglacial cycle from Lake Ohrid, Albania and
1026 Macedonia. Journal of Paleolimnology 44, 295–310.

1027 Vogel, H., Meyer-Jacob, C., Thöle, L., Lippold, J.A., Jaccard, S.L. (2016). Quantification of biogenic
1028 silica by means of Fourier transform infrared spectroscopy (FTIRS) in marine sediments. Limnology &
1029 Oceanography: Methods, *in press*. doi: 10.1002/lom3.10129

1030 Wehausen, R., Brumsack, H.J., 1999. Cyclic variations in the chemical composition of eastern
1031 Mediterranean Pliocene sediments: a key for understanding sapropel formation. Marine Geology 153 (1–
1032 4), 161–176.

1033 Wierzbowski, H. 2007. Effects of pre-treatments and organic matter on oxygen and carbon isotope
1034 analyses of skeletal and inorganic calcium carbonate. International Journal of Mass Spectrometry 268,
1035 16–29.

1036 Wold, S., Sjöström, M., Eriksson, L. 2001. PLS-regression: a basic tool of chemometrics. Chemometrics
1037 and intelligent laboratory systems 58(2), 109-130.

1038 Wulf, S., Keller, J., Paterne, M., Mingram, J., Lauterbach, S., Opitz, S., Sottili, G., Giaccio, B., Albert,
1039 P., Satow, C., Viccaro, M., Brauer, A. 2012. The 100-133 record of Italian explosive volcanism and
1040 revised tephrochronology of Lago Grande di Monticchio. Quaternary Science Reviews 58, 104-123.

1041 Yancheva, G., Nowaczyk, N.R., Mingram, J., Dulski, P., Schettler, G., Negendank, J.F.W., Liu, J.,
1042 Sigman, D.M., Peterson, L.C., Haug, G.H. 2007. Influence of the intertropical convergence zone on the
1043 East Asian monsoon. Nature 445 (7123), 74–77.

1044 Zanchetta, G., Bonadonna, F.P., Leone, G., 1999. A 37-meter record of paleoclimatological events from
1045 stable isotope data on molluscs in Valle di Castiglione, near Rome, Italy. Quaternary Research, 52, 293-
1046 299.

1047 Zanchetta, G., Drysdale, R.N., Hellstrom, J.C., Fallick, A.E., Isola, I., Gagan, M., Pareschi, M.T. 2007a.
1048 Enhanced rainfall in the western Mediterranean during deposition of Sapropel S1: stalagmite evidence
1049 from Corchia Cave (Central Italy). Quaternary Science Review 26, 279-286.

1050 Zanchetta G., Borghini A., Fallick A.E., Bonadonna F.P., Leone G. 2007b. Late Quaternary
1051 palaeohydrology of Lake Pergusa (Sicily, southern Italy) as inferred by stable isotopes of lacustrine
1052 carbonates. Journal of Paleolimnology, 38, 227-239.

1053 Zanchetta, G., van Welden, A., Baneschi, I., Drysdale, R.N., Sadori, L., Roberts, N., Giardini, M., Beck,
1054 C., Pascucci, V. Sulpizio, R., 2012. Multiproxy record for the last 4500 years from Lake Shkodra
1055 (Albania/Montenegro). Journal of Quaternary Science 27, 780-789.

1056 Zanchetta, G., Bar-Matthews, M., Drysdale, R.N., Lionello, P., Ayalon, A., Hellstrom, J.C., Isola, I.,
1057 Regattieri E. 2014. Coeval dry events in the central and eastern Mediterranean basin at 5.2 and 5.6 ka
1058 recorded in Corchia (Italy) and Soreq caves (Israel) speleothems. Global and Planetary Change 122
1059 (2014) 130–139.

1060 Zanchetta, G., Regattieri, E., Isola, I., Drysdale, R.N., Bini, M., Baneschi, I., Hellstrom, J.C. 2016a. The
1061 so-called “4.2 event” in the central Mediterranean and its climatic teleconnections. Alpine Mediterranean
1062 Quaternary 29 (1), 5 –17.

1063 Zanchetta, G., Regattieri, E., Giaccio, B., Wagner, B., Sulpizio, R., Francke, A., Vogel, L.H., Sadori, L.,
1064 Masi, A., Sinopoli, G., Lacey, J.H., Leng, M.L., Leicher, N. 2016b Aligning MIS5 proxy records from
1065 Lake Ohrid (FYROM) with independently dated Mediterranean archives: implications for core
1066 chronology. Biogesciences 13 (9), 2757-2768.

1067

Figures

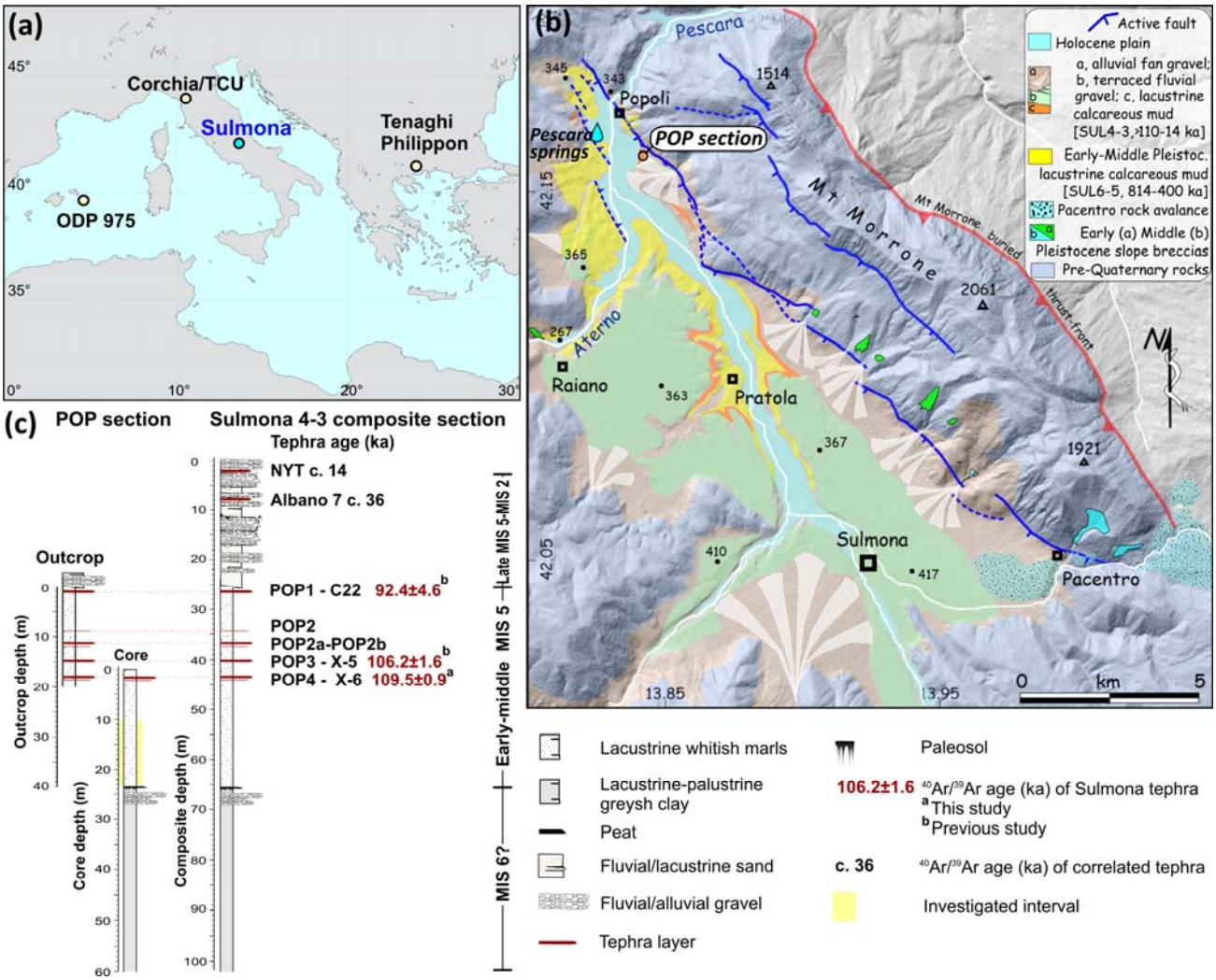

Figure 1- Reference maps of the investigated sedimentary succession. (a) Location of the Sulmona Basin and other sites mentioned in the text; (b) Simplified geological map of Sulmona Basin with the location of the POP section investigated here (from Galli et al., 2015). (c) Lithostratigraphy and tephrochronology of the POP section and of the whole composite section of SUL4-3 unit; NYT: Neapolitan Yellow Tuff.

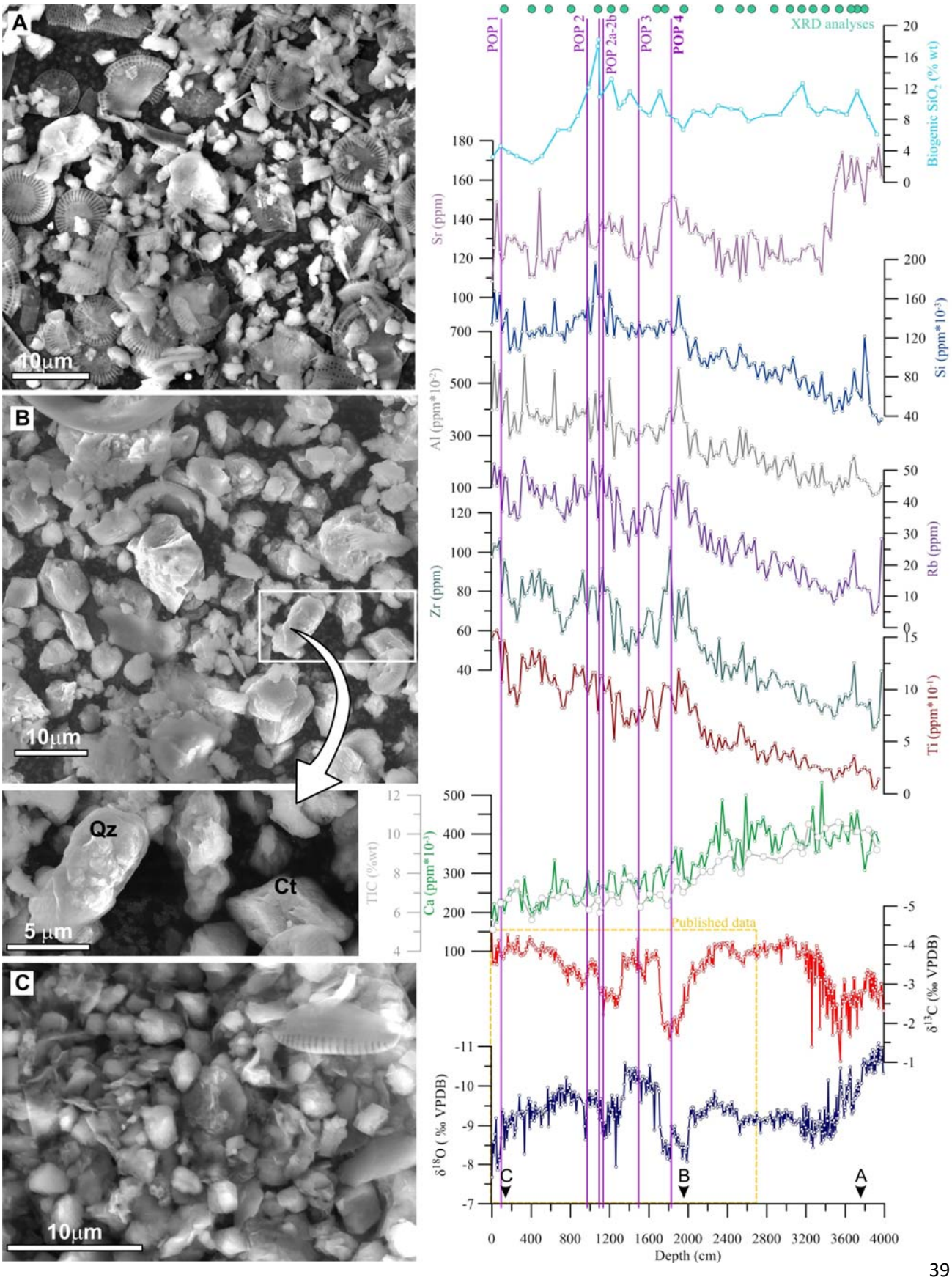
A
10µm
B
10µm
Qz
Ct
5 µm
C
10µm
POP 1
POP 2
POP 2a-2b
POP 3
POP 4
XRD analyses
Biogenic SiO2 (% wt)
Sr (ppm)
Si (ppm*10-3)
Al (ppm*10-2)
Rb (ppm)
Zr (ppm)
Ti (ppm*10-1)
TIC (%wt)
Ca (ppm*10-3)
Published data
δ13C (‰ VPDB)
δ18O (‰ VPDB)
C
B
A
Depth (cm)

1077 Figure 2- Left panel: POP stable isotope, trace element, mineralogical and organic carbon results plotted
1078 vs. depth. From bottom: $\delta^{18}O$ and $\delta^{13}C$ (within yellow box stable isotope data already published by
1079 Regattieri et al., 2015); Ca and Total Inorganic Carbon (TIC), Ti, Zr, Rb, Al, Si, Sr (XRF data converted
1080 to ppm), biogenic silica (% total weight). Purple lines represent tephra layers. The position of XRD
1081 analyses (green dots on top) and of Field Emission Scanning Electron Microscopy FESEM pictures
1082 (letters) is also shown. Right panel: FESEM images of selected samples.

1083

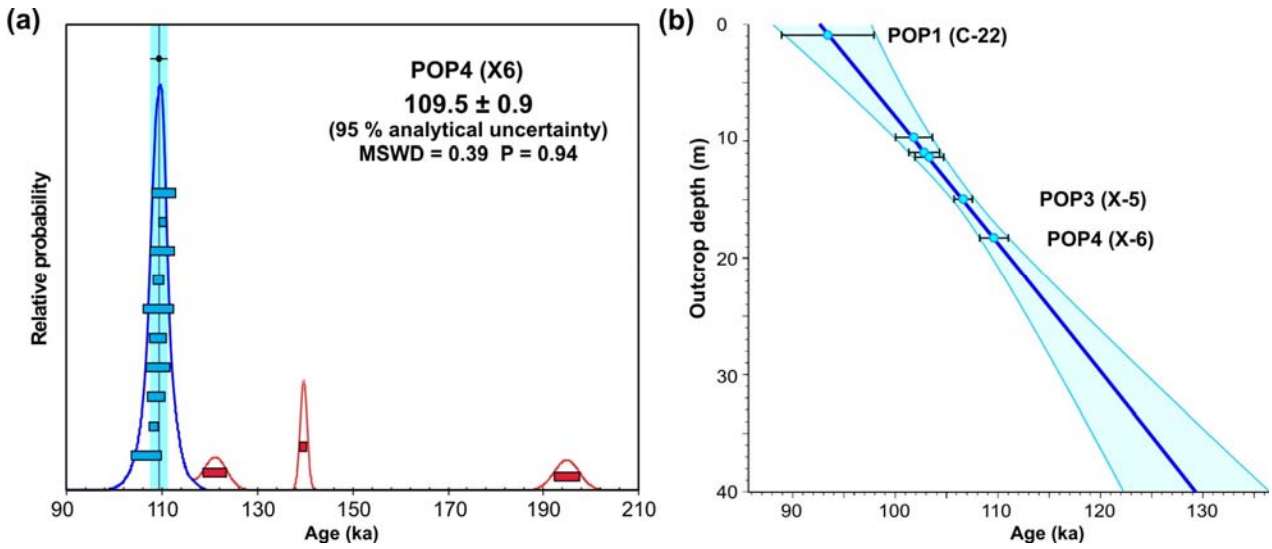

1084

1085 Figure 3- A) Age probability density spectra for the POP4 tephra. Blue and red bars are the individual
1086 ages (1σ error) included and not included in the weighted mean age calculation, respectively; B) Age-
1087 depth model and tephra control points for the POP succession. Blue line indicates the modelled median
1088 age and light-blue lines indicate 95% confidence limits. All tephra ages are modelled ages (see Table 1).

1089

1090

1091

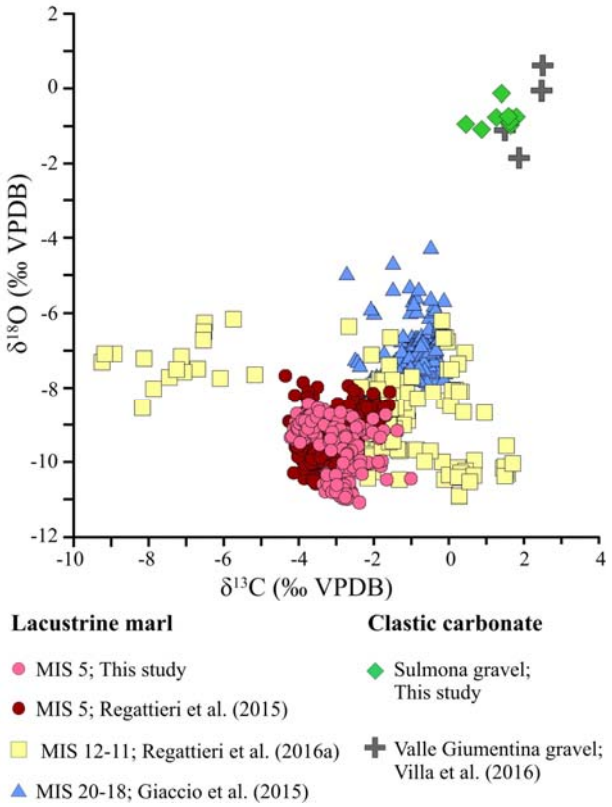

Figure 4- Comparison of stable isotope values from Sulmona lacustrine sediment (pink/red dots: MIS5 samples, the present study and Regattieri et al. (2015) respectively; yellow squares: MIS12-11 samples from Regattieri et al. (2016a); blues triangles: MIS19-18 interval, Giaccio et al. (2015)) and bedrock-clastic material (grey crosses: Sulmona gravels; green diamonds: alluvial sediments from Valle Giumentina (Abruzzo, Villa et al., 2016)).

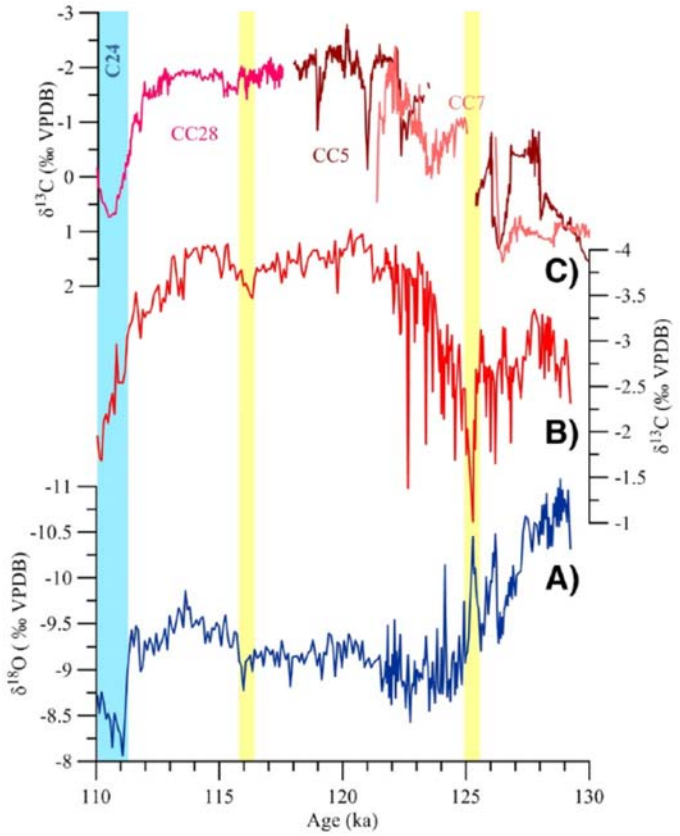

1102

1103 Figure 5- POP stable isotope results plotted vs. age. A) $\delta^{18}O$, B) $\delta^{13}C$ (red). $\delta^{13}C$ composition of
1104 speleothems (CC5, CC7 and CC28) from Corchia Cave (Drysdale et al., 2007, 2009, C). Yellow bars
1105 indicate events discussed in the text and blue bar indicates the event C24 (as defined on POP succession
1106 by Regattieri et al., 2015).

1107

1108

1109

1110

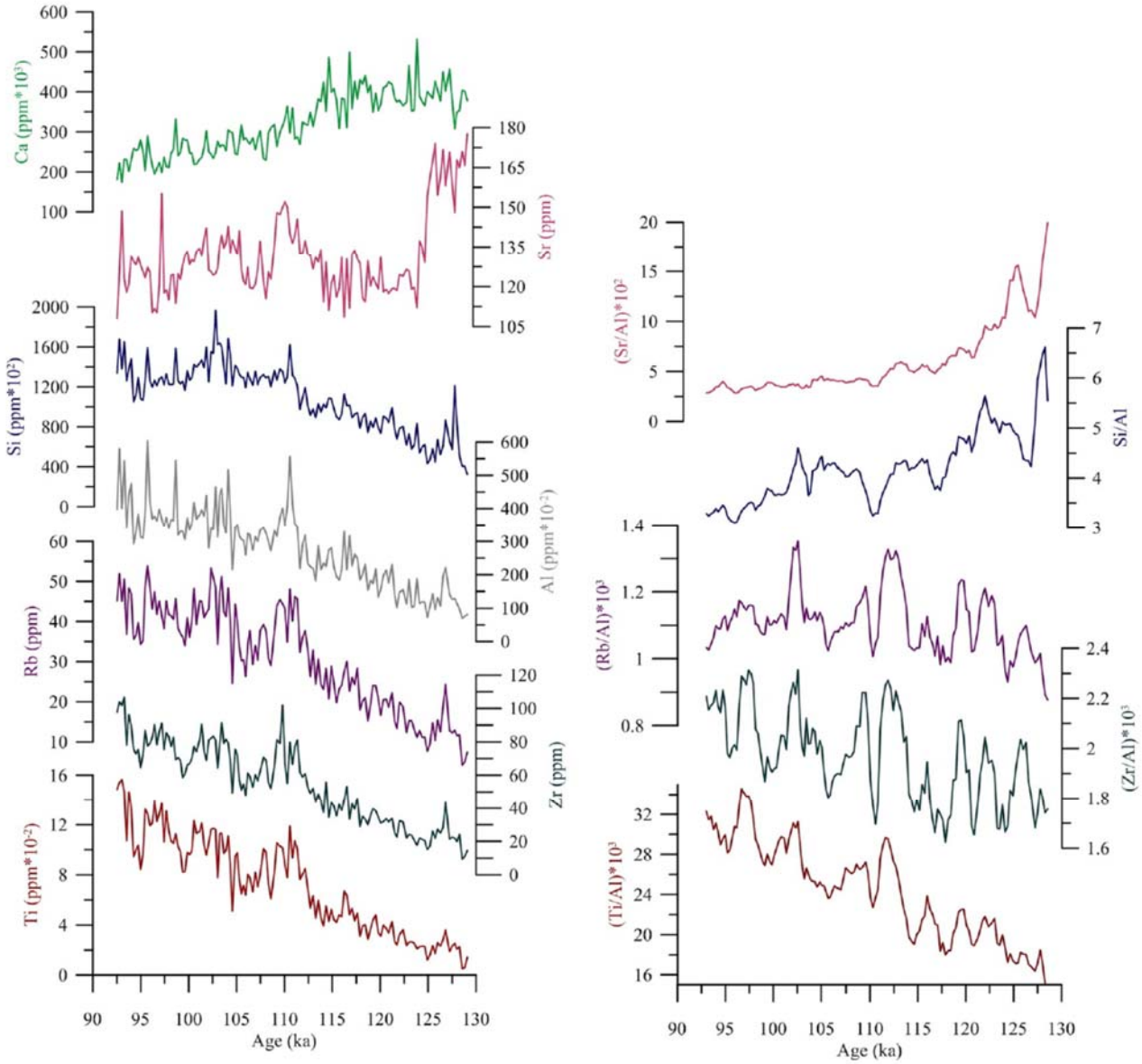

1111

1112 Figure 6- Left panel: XRF results plotted vs. age (from bottom: Ti, Zr, Rb, Al, Si, Sr, Ca); right panel:
1113 Five-point smoothed time series of normalized XRF data (from bottom: Ti/Al, Zr/Al, Rb/Al, Si,/Al,
1114 Sr/Al).

1115

1116

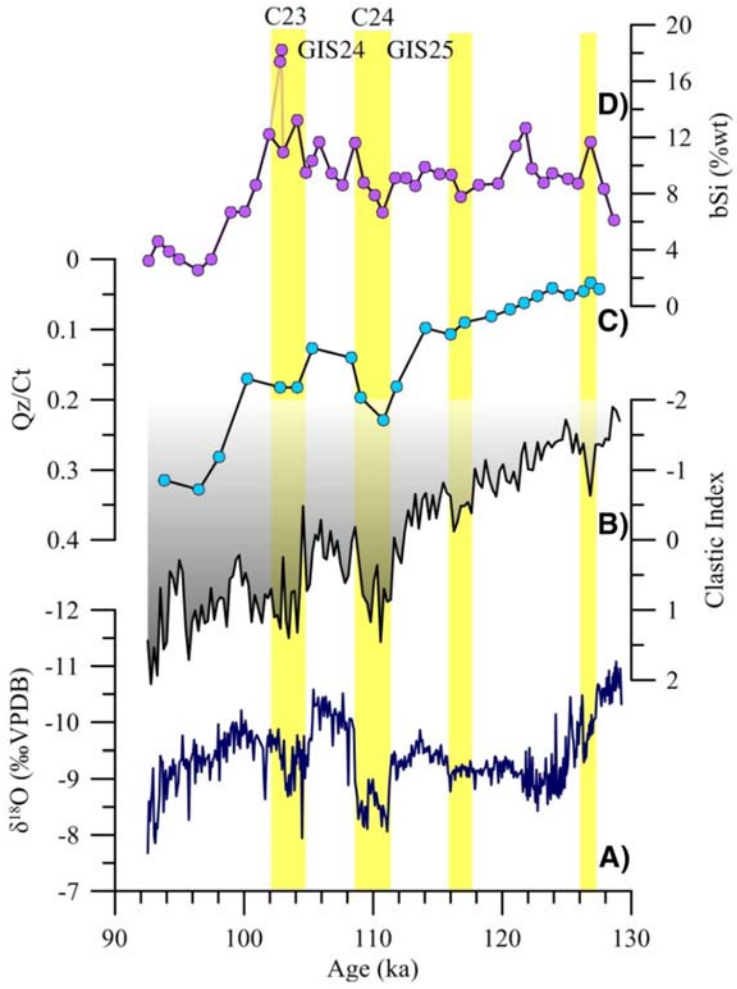

Figure 7 –Comparison of $\delta^{18}O$ (A); Clastic index (CI, see text for explanation; B); quartz/ calcite ratio (Qz/Ct, C) and biogenic silica (bSi, D) time series. Yellow bars indicate dry events discussed in the text, GS are Greenland interstadial, as defined in the POP section by Regattieri et al. (2015)

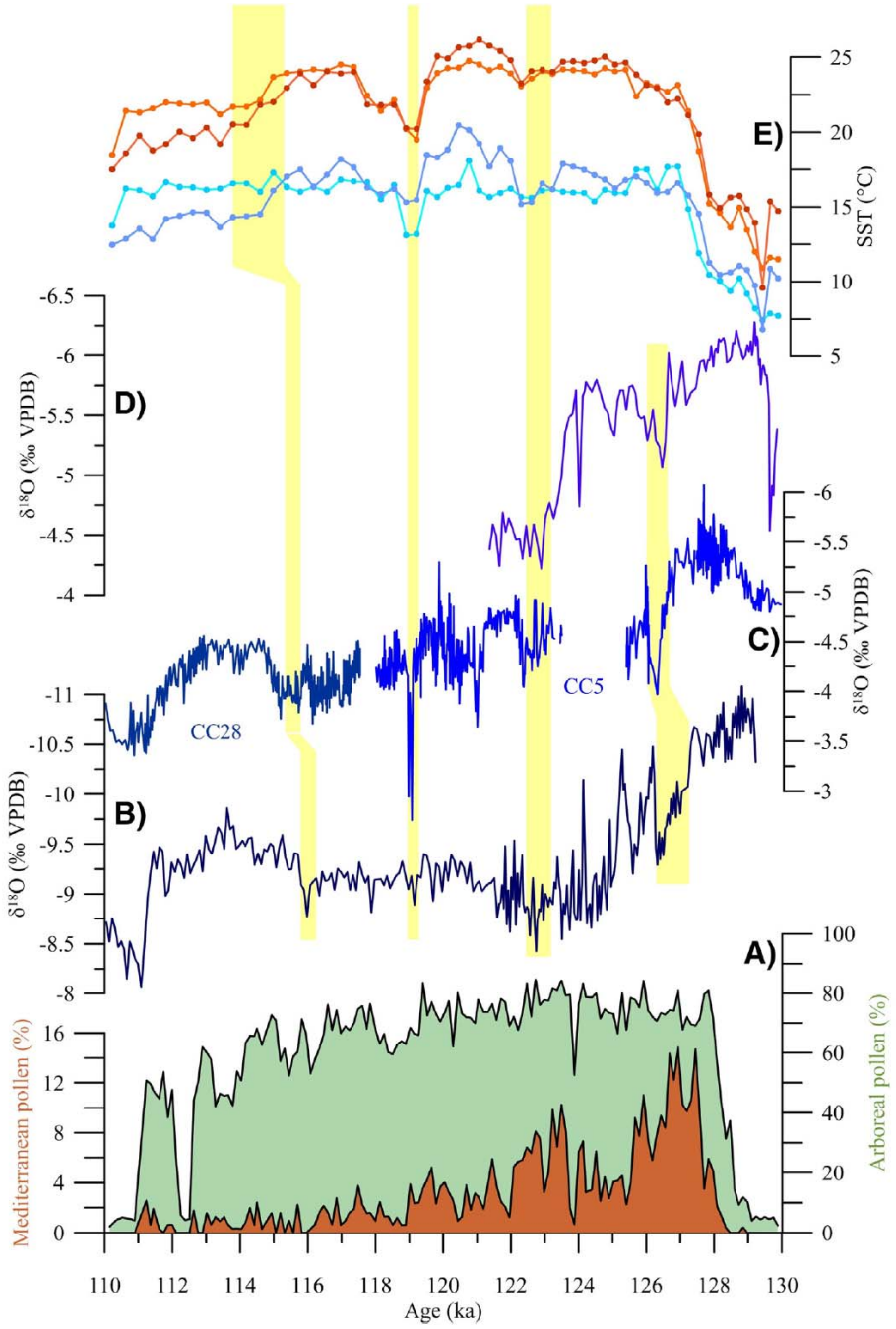

Figure 8- Comparison of POP and regional palaeoclimate records. a) Tenaghi Philippon pollen record (Milner et al., 2013); b)POP $\delta^{18}O$ record; c) Corchia Cave $\delta^{18}O$ record (stalagmite CC28, Drysdale et al., 2007, stalagmite CC5, Drysdale et al., 2009); d) $\delta^{18}O$ record from Tana che Urla Cave (Regattieri et al., 2014a); e) faunal SST record from core ODP-975 (orange, summer temperature; blue winter temperature, lighter lines are from Modern Analogue technique and darker from Transfer Function technique,

Kandiano et al., 2014). Yellow shadings indicate events of reduced precipitation and environmental deterioration. All the compared records are plotted on their published age model.

Sulmona POP section			Monticchio record	Marine record	POP age model (ka) ± 2σ	
Tephra	Depth (m)	$^{40}Ar/^{39}Ar$ age (ka) ± 2σ uncertainty	Tephra	Tephra	Initial age	Modelled age
POP1	0.935	92.4 ± 4.6[a]	TM-23-11	C-22	92.4 ± 4.6[a]	93.4 ± 4.5
POP2	9.690		TM-24-a		101.8 ± 5.0[b]	101.8 ± 1.8
POP2a	10.935		TM-24-b		102.8 ± 5.1[b]	101.4 ± 1.5
POP2b	11.335		TM-24-3b	C-26	104.0 ± 1.0[b]	103.3 ± 1.4
POP3	14.935	106.2 ± 1.3[a]	TM-25	C-27/X-5	106.2 ± 1.3[a]	106.6 ± 0.9
POP4	18.260	**109.5 ± 0.9**[c]	TM-27	C-31/X-6	**109.5 ± 0.9**[c]	109.6 ± 1.4

Reported in bold the new $^{40}Ar/^{39}Ar$ for X6 layer
Tephra ages from:
[a] Giaccio et al. (2012).
[b] Wulf et al. (2012).
[c] The present study.

Table 1- Tephra ages and correlations between POP, Monticchio (Brauer et al., 2007; Wulf et al., 2012) and Mediterranean marine (Keller et al., 1978; Paterne et al., 2008) tephra as proposed by Giaccio et al. (2012) and Regattieri et al. (2015). The resulting modelled tephra ages obtained by the Clam algorithm (Blaauw, 2010) are also shown.

	Ca					
Sr	+0.17	Sr				
Ti	−0.85	−0.29	Ti			
Zr	−0.85	−0.25	+0.98	Zr		
Rb	−0.79	−0.27	+0.96	+0.97	Rb	
Si	−0.67	−0.35	+0.86	+0.86	+0.90	Si
Al	−0.65	−0.29	+0.91	+0.89	+0.93	+0.92

Table 2- Pearson correlation coefficients (r) between elements concentration (XRF data, n=141).

	Zr/Al					
Rb/Al	+0.84	Rb/Al				
Ti/Al	+0.77	0.66	Ti/Al			
K/Al	+0.58	0.67	+0.17	K/Al		
Si/Al	−0.02	0.04	+0.36	+0.49	Si/Al	
Sr/Al	−0.03	0.06	+0.51	+0.48	+0.61	Sr/Al
Ca/Al	+0.19	−0.52	+0.66	−0.47	+0.65	+0.95

Table 3-Pearson correlation coefficients (r) between elements/Al ratios (n=141).

Supplementay figures:

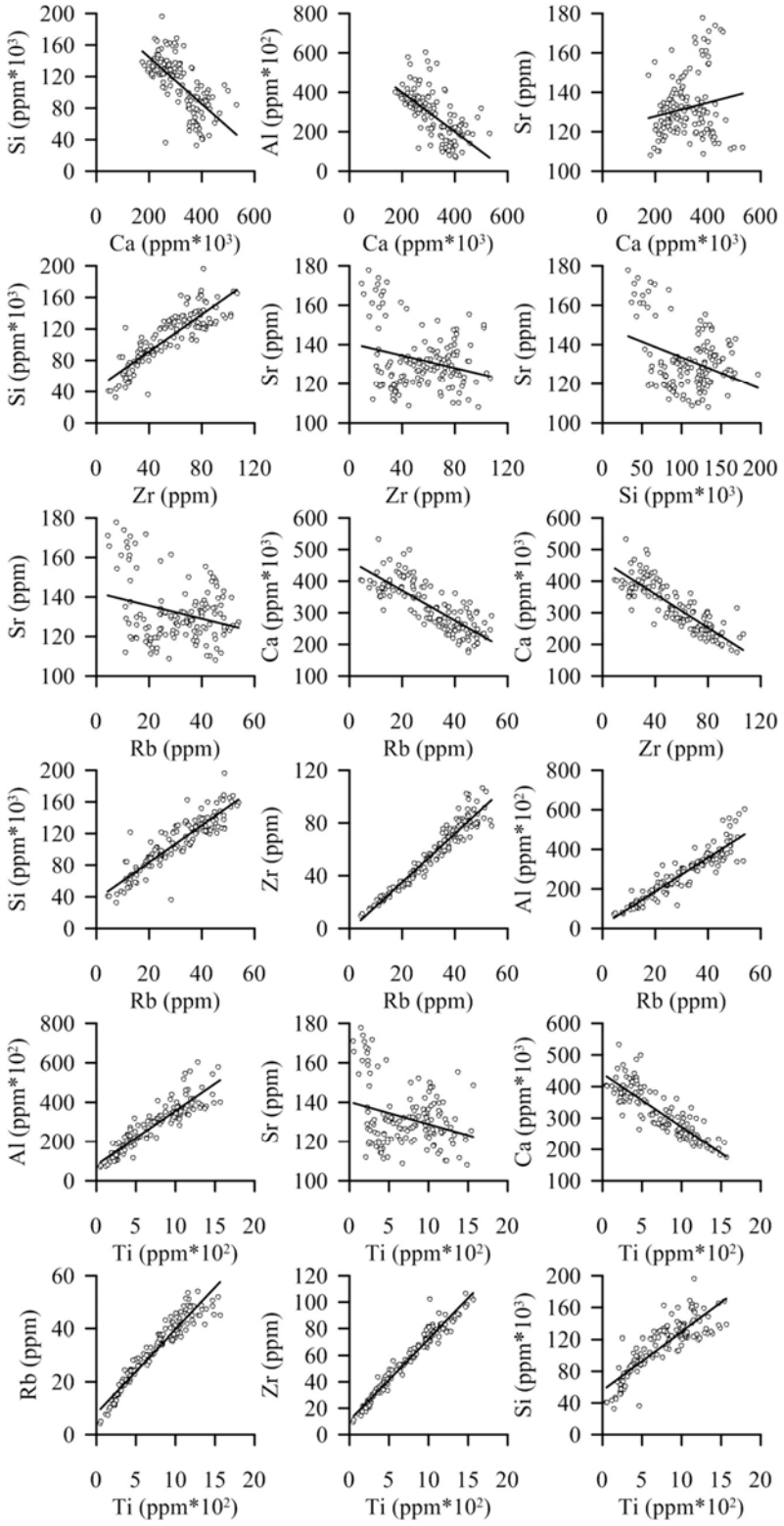

Figure S1- Correlation plots between elements concentrations (XRF data converted to ppm).

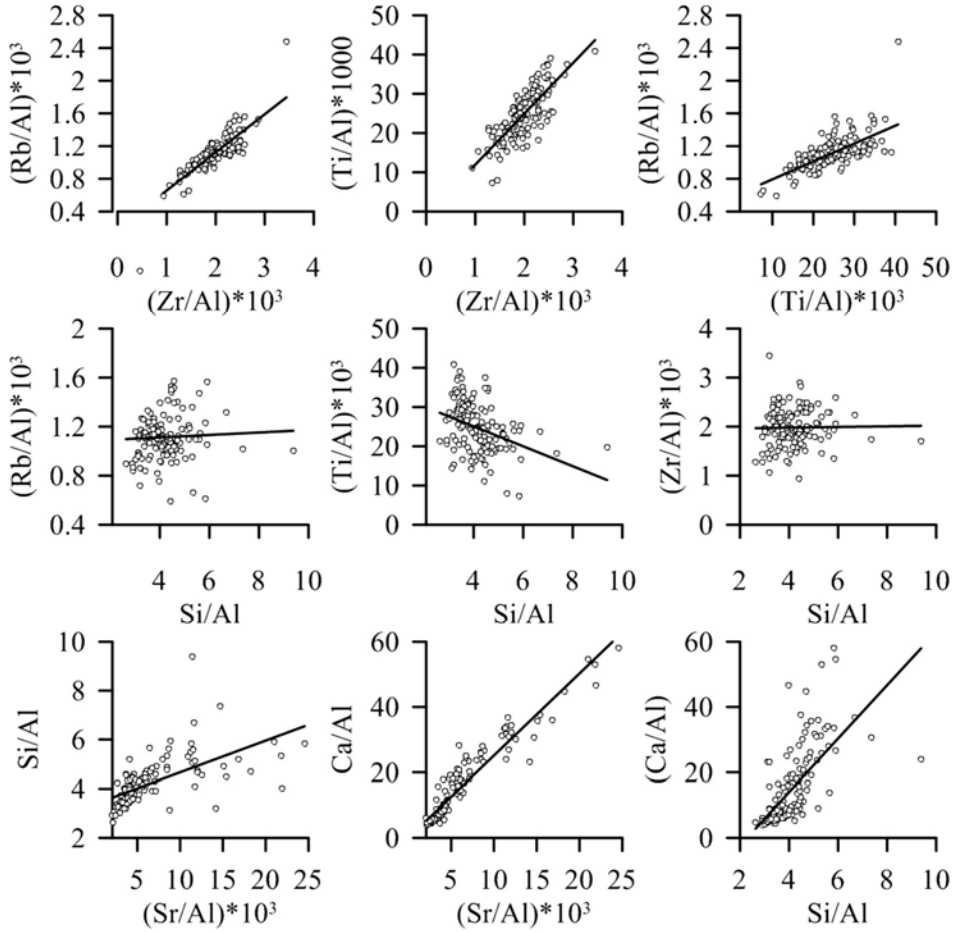

Figure S2- Correlation plots between selected series of elements/Al ratios.

Table S1-Full analytical details for individual crystals of tephra POP4